Advances in Optics and Photonics

Topological photonics in synthetic dimensions

ERAN LUSTIG[1,2] AND MORDECHAI SEGEV[1,2,3,*]

[1]Solid State Institute, Technion, Haifa 32000, Israel
[2]Physics Department, Technion, Haifa 32000, Israel
[3]Electrical Engineering Department, Technion, Haifa 32000, Israel
*Corresponding author: msegev@technion.ac.il

Received December 21, 2020; revised March 30, 2021; accepted March 30, 2021; published June 1, 2021 (Doc. ID 418074)

Topological photonics is a new and rapidly growing field that deals with topological phases and topological insulators for light. Recently, the scope of these systems was expanded dramatically by incorporating non-spatial degrees of freedom. These synthetic dimensions can range from a discrete ladder of cavity modes or Bloch modes of an array of waveguides to a time-bin division (discrete time steps) in a pulsed system or even to parameters such as lattice constants. Combining spatial and synthetic dimensions offers the possibility to observe fundamental and exotic phenomena such as dynamics in four dimensions or higher, long-range interaction with disorder, high-dimensional nonlinear effects, and more. Here, we review the latest developments in using non-spatial dimensions as a means to enhance fundamental features of photonic topological systems, and we attempt to identify the next challenges.

https://doi.org/10.1364/AOP.418074

Topological photonics in synthetic dimensions

ERAN LUSTIG AND MORDECHAI SEGEV

1. INTRODUCTION

1.1 Topological Insulators for Electrons

In the past 15 years, topological insulators have been attracting much research interest in many areas of physics [1–5]. Unlike ordinary materials—conductors, semiconductors, and insulators—topological insulators can conduct on their edges and insulate in their bulk, but what makes them so special is that the current on their edge is completely indifferent to the shape of the material: it is unidirectional (chiral) and robust against most types of disorder. In fact, these materials are considered to be a phase of matter of their own, with features dictated by the topological properties of the conducting and insulating bands that are usually defined on the reciprocal space [6]. Consequently, the bands of topological insulators are classified according to their topology—which is an abstract way to count the number of twists, holes, and other types of geometric features that cannot continuously deform from one to the other. That is, the allowed states for electrons can be classified through topological invariants, determined by externally induced fields or internally through interactions between the particles, and by the structural symmetries in the medium. The first connection between conductance and topology was in the integer quantum Hall effect (IQH) [7]. In the IQH, a magnetic field applied to a 2D electron gas caused its Hall conductance to have integer values. It was then realized that the integer values of the conductance are related to the topology of the allowed states for electrons [6,8,9], and that the classification of the different bands of states is related to robust edge states and a topological invariant called the Chern number [10]. In the following years, it was found that topological insulators can occur even without a net magnetic flux [11] and, even more surprisingly, without any external fields and without even breaking time-reversal symmetry. This happens due to the spin of the electrons themselves (the quantum spin-Hall effect) or via the spin–orbit coupling [4,12,13]. This notion was considered a major breakthrough some 15 years ago since it meant that the properties of topological insulators that were thought to be extrinsic can actually be intrinsic in certain materials. In these intrinsic topological insulators, pairs of edge states related to different spins propagate in opposite directions, but still each one of them is chiral. Moreover, these topological edge states do not couple to each other as long as the time-reversal symmetry is maintained and the gap remains open. In such cases, the topological protection is dependent, in principle, not only on the gap remaining open but also on the existence of a symmetry of the system, in this case: time-reversal symmetry.

These breakthroughs have opened the door for finding many materials with different topological phases of matter with exotic properties. Due to their unique properties, topological materials can potentially be utilized in quantum computing [14], spintronics [15], and more. The relation between topological materials and applications in quantum computing involves additional notions such as fractional Hall states or Majorana fermions that usually require fermionic interactions and, hence, are beyond the scope of this review—which deals mostly with photonics. We are now almost four decades after the discovery of the first topological insulator (the IQH). To understand the underlying principles, it is instructive to briefly review the basics of topological

insulators. We will do it on an intuitive basis and attempt to view these principles through the physically observable quantities. In a single sentence, topological insulators are materials that are insulators in the bulk but are perfect conductors on their edges. The robust conduction on the edge is manifested in the fact that the current there is lossless even in the presence of disorder or defects, and it does not depend on the shape of the edge. That is, the current continues to flow without being scattered into the bulk or being backscattered by local defects, by disorder in the lattice, or by sharp edges. Due to the lack of backscattering, such a topological edge current is often viewed as chiral. This property is often called "topologically protected transport," and it is illustrated in Fig. 1(a). It is this property that made topological insulators so important because—apart from the fundamental physics involved—having a mechanism that can bring lossless flow of energy, charges, or information is extremely important for many applications. The important parameter determining this unique robustness is the strength of the variations of the potential that would have normally caused scattering, not the shape nor the position of a particular defect or disorder in the lattice.

To understand the essence of topological transport, it is instructive to recall the IQH effect [7]. This phenomenon occurs in semiconductors under low temperature and a strong magnetic field [Fig. 1(b)]. The Lorentz force opens a bandgap in the dispersion curve, and the edge states are characterized by a single line crossing the gap in diagonal. This oversimplified picture of the quantum Hall effect is sketched in Fig. 1(c), where the red line marks the dispersion curve of the edge states (in reality, the allowed states form discrete Landau levels separated by bandgaps), and a is the lattice constant. Notice that there is only one line crossing the gap, without any line crossing the gap in the opposite direction. The slope of this line provides the group velocity of any edge excitation (superposition of states on the red line), and it cannot be zero in any topological insulator. The direction of the magnetic field sets the sign of the slope (which determines the direction of the edge current), and the strength of the magnetic field sets the size of the bandgap. Now, if disorder is introduced into this structure, the bands will be slightly modified, and the slope of the red line will be slightly altered. But, as long as the strength of the disorder (random variation in the potential) is smaller than some value, scattering will not couple the edge states to bulk states. The implication is that disorder weaker than (approximately) the width of the bandgap will not cause any scattering into the bulk or backscattering [16]. This is the origin of topologically protected transport in the IQH effect, and its key ingredient is the size

Figure 1

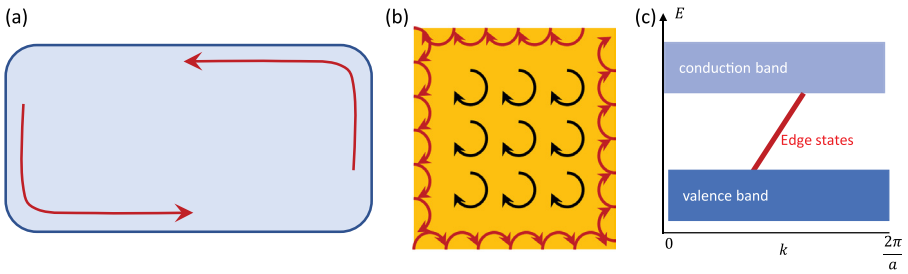

Topological insulators in a nut shell. (a) Topological insulator in two dimensions: a 2D material that is insulating in the bulk but exhibits perfect conduction on the edge. (b) Simplified sketch of the integer quantum Hall effect, which was the first topological insulator. The arrows indicate the cyclotronic movement of electrons induced by a magnetic field perpendicular to the plane. (c) Simplified dispersion relation for the quantum Hall effect, with the red line marking the topological edge states.

of the topological bandgap, which determines the degree of topological protection of transport. More details about the calculation of basic topological invariants are provided in Section 5. Modern topological insulators rely on the same principles, but the effects can be caused by a variety of other sources, among them fermionic spin–orbit coupling, external modulation, and crystal symmetries. These different mechanisms that can give rise to topological insulators may affect the level and type of protection of the edge states, making some more limited than others. The full description of all the different kinds is beyond the scope of this review; therefore, we will mostly use the simplest kind of topological phases to explain the concepts of topological photonics in synthetic dimensions. However, these concepts apply to all types of topological insulators. For a thorough derivation on topological insulators, we direct the reader to one of many reviews that focus on topological insulators and topological phases [17].

1.2 Photonic Topological Insulators

After the discovery of topological insulators, it became evident that topological phases are not unique to electronic materials. In fact, the topological structure of the allowed states for electrons giving rise to the robust edge conductance can occur also for bosonic particles, i.e., photons, phonons, and atoms.

Effectively, the only requirement from a system to present topologically protected transport is to have a dispersion curve resembling Fig. 1(c), with the edge states crossing the gap diagonally. Fulfilling this requirement in bosonic systems implies that topological physics is not unique to fermions and is not in itself a quantum phenomenon. It is a wave phenomenon (because interference is at its heart) that can, in principle, occur in any wave system—classical or quantum—with a judiciously engineered potential landscape [18]. The first suggestion for a bosonic topological insulator was an electromagnetic (EM) system that required breaking time-reversal symmetry to avoid backscattering [19]. Shortly thereafter, a more concrete idea was proposed [20]—based on gyro-optics materials where the application of a magnetic field indeed breaks time-reversal symmetry. This effect is fundamentally weak at all frequencies above THz; hence, the resultant topological bandgap would be very small, providing essentially no protection of transport. However, at microwave frequencies, the effect is strong and opens a large bandgap, and indeed, within a year, the EM analogue of the IQH effect was demonstrated [21]. At that point, the challenge was to find a new avenue to bring the concepts of topological insulators into photonics (optical and near infrared frequencies), without relying on the weak gyro-optic effects. Several ideas were proposed—ranging from using polarization as spin in photonic crystals [22] and aperiodic coupled resonators [23] to bianisotropic metamaterials [24]. Eventually, in 2013, the first photonic topological insulators were demonstrated [25], and they indeed displayed topological protection of transport (of light) against defects and disorder. Around the same time, the aperiodic coupled resonator system was also realized in experiment [26] and a year later demonstrated topological protection against disorder in the lattice [27]. Within a few years, numerous other EM topological systems were proposed and demonstrated, among them the topological bianisotropic metamaterials system [28], the so-called "network model" of strongly coupled resonators [29–31], the crystalline topological insulator [32–36], and the valley-Hall scheme [37–39]. A contemporary review on photonic topological insulators can be found in [40,41].

1.3 Role of Dimensionality and Connectivity in Topological Physics

All the topological photonics work described above was on 2D topological systems, but this is more than a mere coincidence [42–44]. Although a large number of fundamentally different topological phases and topological insulators do exist also for

three dimensions [2–4,12,17] or more than three dimensions [45–49], these phases are very hard to realize in photonic systems. This means that, in all our efforts so far with traditional photonic lattices and structures, we were always only examining the tip of the iceberg, in terms of the diversity of topological phases with different properties. The reason is twofold: First, photons propagate at the speed of light; thus, in the direction of their propagation, it is hard to induce the complex dynamics necessary for topological phases in high dimensions. The second reason is the complexity of fabricating 3D topological structures, such as the 3D structures that were recently used for demonstrating Weyl points [50–52] and the 3D topological insulator in the microwave regime using magneto-optic effects [53]. 3D fabrication becomes much more complicated for higher frequencies in the optical regime, where the length scales are much smaller (implying that higher resolution in fabrication is crucial) and magneto-optic effects are very weak. Of course, systems of dimensions higher than three cannot be fabricated directly and require special approaches.

Another aspect in which most photonic topological structures are limited is their connectivity. Designing a photonic structure that corresponds to a topological phase usually requires the construction of a lattice, which is a periodic arrangement of optical elements in space [54–57]. Generally, lattices play an important role in many topological insulators, as the symmetries and the parameters of the lattice dictate the topological behavior directly. Since our world has only three spatial dimensions, and the coupling between sites is mostly by proximity, this limits the number of possible topological geometries and consequently possible topological phases [11,58], as much as it does for the topological insulators found in condensed matter. That is, the possibility of coupling two sites (or elements) that are far apart from one another is limited in traditional photonic structures, which typically rely on evanescent coupling. We stress that this problem of connectivity is not limited to high-dimensional systems nor to photonics; it is a limitation common to all physical systems in real space and in any dimension. Thus, a possible way to conclude the discussion so far could have been that the major limiting factor in experimentally realizing lattice models in high dimensions and with long-range connectivity is the traditional approach in which lattice sites are identified by their location in space. Luckily, it turns out that this does not have to be the case: it is possible to utilize non-spatial degrees of freedom such as spin, momentum, energy, and time as "lattice degrees of freedom" [59–63]. These non-spatial degrees of freedom are called "synthetic dimensions," and they are not restricted by spatial proximity; therefore, they offer new possibilities in experimentally realizing topological phases that have thus far never been observed. Indeed, recent years have witnessed the use of synthetic dimensions as a means to realize novel topological phenomena in photonics, and even promising avenues to utilize this concept for future applications. In this paper, we review the latest advancements on topological photonics utilizing synthetic dimensions. We explain the fundamental science underlying the ideas of synthetic dimensions in photonics, and we describe the current three leading techniques for realizing synthetic dimensions and the recent experimental efforts. Finally, based on the current state of the research, we map future directions and possible applications for synthetic dimensions in photonics, and we suggest some visionary ideas that may open new avenues in untraditional paths.

1.4 Historic Development of Synthetic Dimensions in Photonics

Using non-spatial degrees of freedom as an auxiliary avenue to observe phenomena that are usually studied in spatial degrees of freedom can be traced back to works on Anderson localization and quantum chaos from the early 1980s in the theory of kicked rotors [64–66]. This approach was suggested later on as a means for experiments in cold atoms [67–70] and also for observing high-dimensional topological

phases [71]. In photonics, however, modulating effectively the dielectric properties of a medium at frequencies comparable to that of the EM field passing through it (as in the kicked rotor approach) is very challenging for frequencies of THz and higher. As a consequence, using synthetic dimensions in photonics has evolved in different avenues, initially relying on a big advantage that photonic systems have on most other areas: the ability to fabricate and engineer large photonic systems with elaborate architectures. However, as the technology evolved, temporal modulation has also been incorporated in implementing synthetic dimensions in photonics. In light of the many different experimental approaches known today, it would seem that using synthetic dimensions to study high-dimensional or more complex topological phases than what the spatial dimensions allow is a multifaced challenge. However, as we show in Section 5 below, there is a uniting underlying logic behind all the approaches for synthetic space topological photonics.

As mentioned earlier, the non-spatial degrees of freedom can take several forms in photonics. Currently, the implementation of synthetic dimensions in photonics can be cast into three main classes. The **first class**, which may be called **"parametric synthetic dimensions,"** is using a parameter of the Hamiltonian, which, when varied (either continuously or in discrete steps), can constitute a "parametric synthetic dimension." However, if the parameter is constant or is varied adiabatically—it lacks a kinetic term. The absence of a kinetic term means that there is no transport in this parametric synthetic dimension. Such systems are simpler to implement compared to other approaches, and they do allow for observing higher dimensional physics in lower dimensional systems, which made them a useful tool. For example, by mapping a 1D lattice to a slice in a 2D model, topological Thouless pumping was demonstrated in photonics experiments [61], and more recently higher dimensional topological pumps were demonstrated in both optics and cold atoms [72,73]. In fact, a recent theoretical proposal suggested systems simulating 6D topological pumps [74]. Other aspects related to topology, such as Fermi arcs and Weyl points, were also demonstrated by exploiting parameter space [75]. Using parameters as synthetic dimensions in topological photonics is explained in Section 2 below.

The second class of non-spatial degrees of freedom may be called "**eigenstates ladder**." It does have a kinetic term in the Hamiltonian that results in propagation along the synthetic dimension; hence, it is considerably richer because it facilitates transport in the synthetic dimensions (which the "parametric synthetic dimensions" simply do not have). In this "eigenstates ladder" class, the synthetic dimensions can be a series of states such as spin states, momentum states, or a train of frequencies, which in principle is a ladder of states. The ladder is an uncoupled lattice, and initially the degree of freedom associated with the ladder does not have a kinetic term, but—with an additional resonant external modulation—the states become coupled; thus, the system becomes endowed with an additional kinetic term in the Hamiltonian [60]. Although modulation for photons can be more complex, and certainly adds complexity (compared to the approach that uses a static parameter as a synthetic dimension), the fact that the modulation is resonant relaxes the conditions for the strength of the modulation. What makes this approach very appealing for realizing topological phases is that a spatially dependent modulation phase is equivalent to imprinting an effective gauge field, which can act on the waves evolving in the system [62]. This artificial gauge field can be engineered by choosing the modulations scheme. Indeed, this approach was used in demonstrating the first topological edge states in cold atoms. There, the synthetic dimensions were spin states, and the coupling between the states was implemented with an external laser [76,77]. Soon thereafter, similar ideas of coupling other degrees of freedom in cold atoms, such as optical lattice clocks [78] and atomic momentum states [79,80], were used in exploring topological phenomena.

The downside of all of these is that the number of spin states and momentum states is small, and generally excited states have a short lifetime, which altogether limit the actual size of the synthetic dimension. But a more recent suggestion—of using modes of a periodically shaken harmonic trap [81]—could, in principle, overcome those limitations.

Slightly after the suggestion for implementing topological physics by utilizing synthetic dimensions with cold atom systems [51], several groups proposed using this concept in photonics. These groups suggested the use of a ladder of resonator modes [82–84], coupled by external modulation, for inducing photonic artificial gauge fields. And, more recently, photonic waveguide modes coupled by spatial modulation with a spatially varying phase were employed to demonstrate the first photonic topological insulator utilizing synthetic dimensions [85]. In a similar vein, magnetic fields in synthetic dimensions were experimentally demonstrated in microwaves [86] and on a single resonator with two independent mode ladders in optical wavelengths [87,88]. These ideas, together with suggestions to exploit synthetic dimensions for generating higher dimensional topological phases [83,89,90] and high-order topological phases [91], have recently become promising avenues for future research, together with novel applications employing topologically protected edge transport for robust unidirectional frequency conversion [92] and mode-locking an array of laser emitters [93]. We discuss this approach in Section 2 below. Another advantage in coupling ladders of modes as synthetic dimensions is the ability to couple modes that are not close to one another. In this way, using synthetic dimensions can be designed to introduce long-range coupling, which offers a means not only to enrich the topological phases [94] but also to increase their fundamental dimensionality [95]. In fact, using long-range connectivity can be a type of synthetic dimension of its own, as was proposed already in 2013 [63] in the context of demonstrating high-dimensional optical solitons, and it was recently used to demonstrate experimentally 4D topological phases in a circuit implementation [96]. Furthermore, coupling synthetic degrees of freedom does not necessarily require active modulation. A static geometry can also induce a topological model utilizing synthetic dimensions by transforming not to an eigenstate basis but to a non-diagonal basis [97–99].

Finally, the third approach for introducing a synthetic dimension has to do with discrete dynamics in a synthetic space of "time-bins." This approach employs laser pulses propagating in a periodic cycle. At each period, each pulse splits into several consecutive pulses, such that they arrive to the measurement device at different times—due to different delay for each pulse. Each time slot of arrival ("time-bin") is analogous to a location in space. In this approach, the light changes its location (which is the time-bin) constantly; therefore, this approach is endowed with a kinetic term and displays transport in the synthetic dimension. Unlike the first two approaches, here the propagation is only sampled at discrete times, associated with the steps of a discrete time quantum walk (DTQW). Quantum walks have been known for almost three decades to be a useful tool for studying a plethora of quantum and wave phenomena [100–104]. In photonics, DTQWs were experimentally realized with short pulses in fiber loops [105] and allowed the experimental realization of phenomena such as parity–time (PT)-symmetric lattice [59], Kapitza light guiding [106], time-reversed light [107], optical diametric drive [108], and more [109–112].

A decade ago, along with the growing interest in topological phases of matter, it was realized that DTQW can exhibit topological phases, not only in 1D but also in higher dimensions [113]. At first, 1D topological phases and topological edge states in DTQW were experimentally demonstrated in photonics in several platforms [114–118]. The 1D topological phases in DTQW are now being extended to include

exotic phenomena such as non-Hermitian topological edge states [119] and observation of the topological funneling of light in a non-Hermitian topological DTQW [120]. In parallel, experimental efforts to realize 2D (or higher dimensional) synthetic lattice models that can exhibit topological phases are ongoing. Since the basic time-multiplexing system is zero-dimensional, the basic addition of time-bins converts it to 1D only. Topological systems with higher dimensions can take several forms: they can either be further extension of time-bins [121,122], or in combination with other degrees of freedom such as orbital angular momentum [123].

More recently, time-bins were employed to demonstrate unidirectional topological edge states in two dimensions. This was done both by extending the dimensionality of the time-bins to the synthetic dimension [123,124] and by using an additional synthetic dimension of angular momentum modes [125]. This platform is a promising tool to combine synthetic gauge fields [124], non-Hermitian physics [59], and other effects for photons to demonstrate exotic photonic topological phases. We focus on this method and its topological aspects in Section 2 of this review.

2. BASIC PHYSICS OF TOPOLOGY IN SYNTHETIC DIMENSIONS

2.1 Topological Phases and Topological Invariants

The basic notion underlying a phase transition is that physical systems have discontinuous transitions in their properties—upon changing continuously some parameter of the system. The transition between different phases is traditionally described in the Landau framework, where an order parameter of the system changes due to spontaneous symmetry breaking. In recent years, it became evident that a wide class of materials undergo phase transitions called "topological phase transitions" that follow a completely different mechanism. In a topological phase transition, the fundamental property that changes abruptly is the topology of the eigenfunction space of the Hamiltonian. The eigenfunctions are directly deduced from the Hamiltonian, so accordingly the topology is encoded in the Hamiltonian. Topology deals with continuous deformations of abstract structures, and consequently their classification should be according to subspaces in which the structures can deform (transform) from one class of structures into one another without a discontinuity. For example, a sphere cannot deform continuously to a torus since at a certain point the sphere will have to go through a discontinuous transition, which punches a hole into it. Thus, a Hamiltonian with non-trivial topology (such as the toplogy of the torus) cannot deform continuously to a Hamiltonian with a trivial topology, without its subspace of eigenfunctions undergoing some discontinuous transition (example, closing of the bandgap).

When a material (or a system) with non-trivial topology borders a material with different topology (which may be either trivial topology or a different non-trivial topology), the edge between the materials will host edge states with properties different than those of either of the two bulks. Since the two materials (one of which can be vacuum) cannot deform into one another continuously, the deformation occurs only on the edge, which implies that the edge wave functions must be exponentially localized. The properties of the edge states are unique to the edge and depend on the dimensionality, symmetries, and other attributes of the topological system. For concreteness, let us study a Hamiltonian $H(\boldsymbol{k})$ describing a spinless boson on a n-dimensional lattice material, where $\boldsymbol{k}$ is the momentum quantum number, which depends on the space dimensionality, i.e., $\boldsymbol{k}$ is an n-dimensional vector. The Hamiltonian H associates a wave function $\psi(\boldsymbol{k})$ to each $\boldsymbol{k}$ in the Brillouin zone in each band. Thus, the band in a given Brillouin zone, together with the wave function, forms a topological structure. If two materials are in different topological phases, then we cannot continuously

deform the Hamiltonian $H(\boldsymbol{k})$ from one to the other, without closing the gap—which manifests a discontinuous change in the topological structure. For example, if our Hamiltonian describes a 1D dimer (diatomic) lattice, i.e., a 1D lattice that has bonds with strengths alternating between two values (say, u and v, where u is the bond inside the unit cell and v is the bond between unit cells), then there can be two possible topologies ($\mathbb{Z}_2$) [126], where $\mathbb{Z}_2$ symbolizes a set of two integers$\{0,1\}$. These two possible topologies are either a trivial topology ($u > v$), which maps to the topological structure in Fig. 2(a), or a non-trivial topology ($u < v$), which is isomorphic to Fig. 2(b). In Figs. 2(a) and 2(b), the loop maps to the 1D Brillouin zone of the 1D dimer, and the phase of the eigenstates maps to the arrow that winds around the loop. In Fig. 2(a), the arrow does not wind around the loop (trivial), and, in Fig. 2(b), it winds once (non-trivial). The two structures cannot continuously deform to one another and, therefore, are topologically distinct (a structure that winds twice can continuously deform to a structure that does not wind). Mathematically, what classifies the two topological regimes is a topological invariant calculated on the 1D band. In a 1D dimer lattice, the invariant is called the Zak phase, given by

$$\gamma = i \int_k \left\langle \psi(k) \left| \frac{d}{dk} \right| \psi(k) \right\rangle \mathrm{d}k, \tag{1}$$

where the integration is carried out on a 1D band in the Brillouin zone and the Zak phase is equal to 0 or π (indicating the two possible topological phases). As can be seen in Eq. (1), the Zak phase is more general than the dimer case and can be calculated for any 1D lattice. The physical meaning is that, if two 1D lattices with different integer Zak phases border each other, this interface will host an exponentially localized edge state in the gap. From Figs. 2(a) and 2(b) and Eq. (1), we can actually understand that the Zak phase calculates the geometric phase acquired by the wave function when it continuously slides along the Brillouin zone.

Interestingly, the picture looks completely different if we look at different dimensions or different symmetries. For example, for a 2D square lattice with a perpendicular magnetic field (the IQH) [10] or other lattices such as the extended Haldane model [11,58], the topology can potentially be classified not to two subclasses (as in the 1D dimer case) but to infinitely many subclasses identified by integers $\mathbb{Z}$. The topological structures map to structures of 2D vectors on a torus (band in the Brillouin

Figure 2

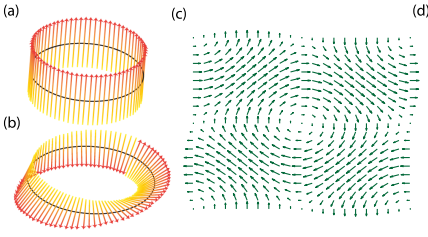

(d)

CL	θ	Ξ	Π	1	2	3	4	5	6	7	8
A	0	0	0	0	$\mathbb{Z}$	0	$\mathbb{Z}$	0	$\mathbb{Z}$	0	$\mathbb{Z}$
AIII	0	0	1	$\mathbb{Z}$	0	$\mathbb{Z}$	0	$\mathbb{Z}$	0	$\mathbb{Z}$	0
AI	1	0	0	0	0	0	$2\mathbb{Z}$	0	$\mathbb{Z}_2$	$\mathbb{Z}_2$	$\mathbb{Z}$
BDI	1	1	1	$\mathbb{Z}$	0	0	0	$2\mathbb{Z}$	0	$\mathbb{Z}_2$	$\mathbb{Z}_2$
D	0	1	0	$\mathbb{Z}_2$	$\mathbb{Z}$	0	0	0	$2\mathbb{Z}$	0	$\mathbb{Z}_2$
DIII	-1	1	1	$\mathbb{Z}_2$	$\mathbb{Z}_2$	$\mathbb{Z}$	0	0	0	$2\mathbb{Z}$	0
AII	-1	0	0	0	$\mathbb{Z}_2$	$\mathbb{Z}_2$	$\mathbb{Z}$	0	0	0	$2\mathbb{Z}$
CII	-1	-1	1	$2\mathbb{Z}$	0	$\mathbb{Z}_2$	$\mathbb{Z}_2$	$\mathbb{Z}$	0	0	0
C	0	-1	0	0	$2\mathbb{Z}$	0	$\mathbb{Z}_2$	$\mathbb{Z}_2$	$\mathbb{Z}$	0	0
CI	1	-1	1	0	0	$2\mathbb{Z}$	0	$\mathbb{Z}_2$	$\mathbb{Z}_2$	$\mathbb{Z}$	0

(a) and (b) Trivial and topological structures of a dimer lattice, respectively, composed of a 1D loop with a vector on each point. The structures are mappings of the topology of a band in a 1D dimer lattice. There are only two distinct topological structures (adapted from [127]). (c) Topological structure of a 2D torus with vector on each point (the projections of the vectors on the plane is presented). This structure is a mapping of the topology of a band in a 2D Chern insulator. (d) "Periodic table" of possible topological phases for quadratic Hamiltonians (see description of the different symmetry classes in [45]).

zone) [Fig. 1(c)]. If we integrate along a loop that encircles the center, we can see that the vector can wind and accumulate a geometric phase when completing the loop. The geometric phase accumulated can only come in integer multiples of 2π, and it is clear from the image why these cannot deform to one another without a discontinuity. Mathematically and more generally, this is calculated by the Chern number. The Chern number calculation is also an integral on the band, but—since this is a 2D band—the integral is carried out over a closed path encircling the Brillouin zone,

$$C = \oint_L \langle \psi(\boldsymbol{k}) | \nabla_{\boldsymbol{k}} | \psi(\boldsymbol{k}) \rangle \, \mathrm{d}\boldsymbol{k}, \tag{2}$$

where L is a closed path in the 2D Brillouin zone. The possible topologies can be any integer $\mathbb{Z}$ depending on the Hamiltonian, and this maps to different discontinuities with different windings around them in Fig. 2(c). We note that the Chern number is not the only topological invariant used to characterize a 2D topological structure; rather, we give it here only because it is a commonly used one. The choice of topological invariants depends on the symmetries and dimensionality of the system, and the Chern number commonly describes the topological structure in models such as the IQH or the Haldane model, where the non-trivial topology arises from broken time-reversal symmetry (driven by the magnetic field, in these cases). Of course, one can go on and describe topological phases in higher dimensions that are described by other structures.

2.2 Richness of Topological Realm

The fact that different dimensionality and different symmetries can lead to completely different topologies raises an important question. What are the possible topological phases for different dimensionalities and Hamiltonian symmetries?

An answer to this question was given in the form of a periodic table for the different possible topological insulating phases. First, for quadratic Hamiltonians, the possible phases were organized according to dimensionality (up to eight dimensions) and non-spatial symmetries, as shown in Fig. 2(d) [45,128]. The different classes (CL) in Fig. 2(d) are composed of different combinations of time-reversal symmetry (Θ), particle-hole symmetry (Ξ), and chiral symmetry (Π), and the symbols ($\mathbb{Z}_2$, $\mathbb{Z}$, $2\mathbb{Z}$, 0) refer to the possible classification for each symmetry class at a certain dimensionality—for example, the IQH model just described is in two dimensions in class A (it is defined with no symmetries), so its topological structures can be classified to an infinite number of topologically distinct phases (for each integer $\mathbb{Z}$). Later on, this table was extended to include also spatial symmetries [129–132]. Current theoretical and experimental efforts are dedicated toward finding topological phases in non-Hermitian systems [133–141] and extending the periodic table [46,142] to include them, likewise with systems of interacting particles [143–145] and nonlinear optics [146,147].

Interesting topological phases in high dimensions also occur not only for insulators but also for semimetals, such as the 5D generalization of the topological Weyl semimetal and more [49]. Of course, dimensionality changes dramatically the properties of the edge states. Just as plain examples, 3D topological insulators include 2D surface currents as edge states [12], while 4D topological insulators can obtain 3D volume edge states [96]. These are of course just examples of the many differences that come about to the different symmetries and topological structures that are made possible by different dimensions.

Since we live in a 3D world, most systems are naturally limited to two or three spatial dimensions. Hence, it became evident that, in order to experimentally study and

fully understand high-dimensional topological phases or complex topological phases that cannot be realized in simple lattices, new experimental approaches should be developed. This was the reason underlying the very large progress on topological physics in synthetic dimensions.

3. DESCRIPTION AND DEFINITION OF NON-SPATIAL DIMENSIONS

An avenue for realizing physical systems with high dimensionality and new forms of lattice connectivity is to use non-spatial degrees of freedom as additional dimensions to the physical system, thus extending the reach of experimental platforms. Examples of non-spatial dimensions are sequences (either discrete or continuous) such as time, energy, spatial frequency, spin, or simply some parameter of the system. Thus, if α is a non-spatial variable associated with the wave function, it has a quantum momentum k_α attached to it, and this pair (α and k_α) can serve as a non-spatial dimension. If the non-spatial dimension α describes a periodic structures, k_α is a quasi-momentum. It is customary to refer to this non-spatial degree of freedom as "synthetic." We note that even if α is a constant parameter, we can still use a notion of an auxiliary Hamiltonian in which α is a variable, and the real Hamiltonian will be a subspace of this auxiliary Hamiltonian. As mentioned, the topology is usually defined on the Brillouin zone, so defining a coordinate k_α is a notion that exists in almost all approaches of topology in synthetic dimensions. An example of an exception to this, which we will not discuss in detail in this review, is the family of topological phases defined in non-periodic systems and is not calculated on the bands in Brillouin zone—for example, quasicrystal, amorphous, or fractal topological systems [56,57,148]. In this case, the synthetic dimensions will only be α, and there is no need for a notion of k_α. In such systems, the Chern number is defined on the real-space structure of the system [rather than the momentum space definition of Eq. (1)], in the thermodynamic limit of a very large system (see discussion in [57]).

The idea is to choose the non-spatial dimension wisely, such that the Hamiltonian $H(\boldsymbol{k}, k_\alpha)$ will describe an extended "Brillouin zone" on the extended momentum space with $n+1$ dimensions (or more generally $n+m$ dimensions, with m being the number of synthetic dimensions). Thus, the eigenstates of $H(\boldsymbol{k}, k_\alpha)$ and the extended Brillouin zone can have topological phases associated with more than n dimensions, which consequently extends the ability of experiments to reach uncharted territories, some predicted by theory and some that were not even theorized.

One might ask at this point, where can this extra dimensionality come from? The answer to this question differs from approach to approach, and even sometimes for different techniques within the same approach. In the case of a synthetic dimension, which is a true internal degree of freedom, such as the polarization of a photon, the answer is straightforward—and it is that the extra dimensionality comes from the conversion of an internal degree of freedom to a spatial degree of freedom. Furthermore, we need to remember that k represents a Bloch lattice momentum—for example, if we have a lattice of ring resonators, then the momentum k only represents a discrete lattice of the position of each ring, but the ring itself has inner spatial complexity (and, therefore, frequency modes) that can be converted (as we will see in Section 3.2) into a ladder of discrete states acting as a spatial axis. This discussion is intended to make clear the obvious reasoning that a synthetic dimension is never "added" to a physical system. That is why, if a constant parameter is used as a synthetic dimension, it will only give access to a small part of the synthetic system, at a given time.

After formulating the Hamiltonian as $H(\boldsymbol{k}, k_\alpha)$, with one or more quantum momentum variables that are synthetic (not a momentum of a real spatial axis), the topological classification and topological invariants are calculated based on this

extended Brillouin zone. For example, the Chern number [Eq. (2)] in a system with one real spatial dimension k_x and a synthetic space dimension k_α is calculated in the following way:

$$C = \oint_{\tilde{L}} \langle \psi(\tilde{\boldsymbol{k}}) | \nabla_{\tilde{\boldsymbol{k}}} | \psi(\tilde{\boldsymbol{k}}) \rangle \mathrm{d}\tilde{\boldsymbol{k}}, \tag{3}$$

where $\tilde{\boldsymbol{L}}$ is a loop on the extended Brillouin zone of $\tilde{\boldsymbol{k}} = (k_x, k_\alpha)$. Since the implications of a non-trivial Chern number in the Brillouin zone are edge states in the space coordinate reciprocal to $\tilde{\boldsymbol{k}}$, when using a synthetic space k_α, the edge states reside on the edge of the synthetic parameter α, which may yield very interesting dynamics when viewed in the complete real-space experimental setup. These special dynamics will be discussed in Section 3.2.

In the next sections, we describe the three leading approaches in constructing synthetic dimensions in topological photonics. As it turns out, while achieving higher dimensionality was the main motivation to use synthetic dimensions at first, it is now clear that the use of non-spatial dimensions is much more than "just" adding dimensionality. Rather, using synthetic dimensions had led to exploring new phenomena such as robust unidirectional transport in non-spatial dimensions, non-local interactions, long-range connectivity, and more. Some of these new ideas were shown to be promising tools not only for basic science but actually also for future technology.

3.1 Topological Photonics in Parameter Space

We begin by describing a synthetic dimension in the form of a static parameter, i.e., a parameter that does not add a kinetic term to the Hamiltonian. In this approach, we treat a static parameter as an additional quantum momentum k_α, and with it we obtain an extended Brillouin zone and higher dimensional topological phases. This method allows for observing phenomena in dimensions higher than the physical dimension of the system they are constructed in, but the lack of kinetic term implies that there is no transport along the synthetic dimensions.

A very elegant example of the idea of synthetic dimensions in parameter space is the use of the 1D Andre–Aubry (AA) model [149]. This is an aperiodic 1D lattice model with non-interacting particles, but it represents a 2D lattice if one of its parameters is treated as the momentum quantum number. As such, the AA model allows for experimentally observing a phenomenon related to 2D topological effects in a 1D lattice—namely, the quantum Hall topological pumping [61]. Extending this approach to a 2D lattice, which is the vector product of two 1D AA lattices, has facilitated observing experimentally 4D topological phenomena in both photonics and cold atoms [72,73], and suggestions for observing 6D topological phenomena are now awaiting to be realized in the lab [74,150]. We will use these examples to explain the ideas underlying synthetic dimensions in parameter space.

The AA model is given by the Hamiltonian,

$$H(n) = \sum\nolimits_n \lambda c_n^\dagger c_n \cos(2\pi b n + \phi) + \left[t c_n^\dagger c_{n+1} + \mathrm{h.c} \right], \tag{4}$$

where c_n ($c_n^\dagger$) is the annihilation (creation) operator related to site n, h.c. is the Hermitian conjugate, and λ, t, ϕ, b are all parameters of the Hamiltonian setting the strength of the coupling and on-site energy in each site in the 1D lattice. Physically, the parameter ϕ relates to the spatial variation of the coupling in some prescribed fashion—it is a parameter of the Hamiltonian. If we treat the parameter ϕ as a quantum number representing the momentum in some auxiliary second dimension m, that is, if $\phi \equiv k_m$, then $H(k_n, k_m)$ becomes the Hamiltonian of a 2D lattice (n, m) with

constant magnetic flux b, where one of its dimensions m has been Fourier transformed to the momentum coordinate k_m. Substituting instead of ϕ, k_m gives

$$H(n, k_m) = \sum\nolimits_n \lambda c_n^\dagger c_n \cos(2\pi bn + k_m) + \left[t c_n^\dagger c_{n+1} + \text{h.c}\right]. \tag{5}$$

Next, we Fourier transform k_m in our synthetic space Hamiltonian of Eq. (5) and obtain the 2D Harper model, describing a square lattice with perpendicular magnetic flux b,

$$H(n, m) = \sum\nolimits_n \lambda e^{i2\pi bn} c_{n,m}^\dagger c_{n,m+1} + t c_{n,m}^\dagger c_{n+1,m}. \tag{6}$$

The Brillouin zone of our fictitious 2D lattice is a surface in the coordinates (k_n, k_m), and due to the magnetic flux b it has a topological invariant—the Chern number [Eq. (2)].

As mentioned earlier, it is clear that 2D photonic systems are easier to fabricate and to control experimentally than 3D ones, but this is not the only reason why using synthetic dimensions increases the experimental possibilities. For example, in the AA model just described, the magnetic field is now included in the parameter b, which represents part of the prescribed spatial variation in the coupling constant. Thus, while effective magnetic gauge fields are very hard to implement for photons in the physical world because photons are non-interacting particles (and, thus, are not affected by free-space EM fields), this model allows us to effectively do this simply by changing the distances between lattice sites.

In the AA model, it is possible to calculate the Chern number in synthetic dimensions with the following expression:

$$C = \oint_{\tilde{L}} \left\langle \psi(\tilde{\boldsymbol{k}}) | \nabla_{\tilde{\boldsymbol{k}}} | \psi(\tilde{\boldsymbol{k}}) \right\rangle \mathrm{d}\tilde{\boldsymbol{k}}, \tag{7}$$

where $\tilde{\boldsymbol{k}} = (k_n, k_m) = (\nu_n, \phi)$, and $\tilde{\boldsymbol{L}}$ is a closed path encircling the extended Brillouin zone in synthetic space.

Importantly, the reason to use synthetic dimensions is to observe physical phenomena that are hard or impossible to realize in a real-space lattice. One such phenomenon, relevant to the Harper model, is called quantum pumping, and it is deeply related to the Chern number and edge states. Quantum pumps are the quantized transformation of wave packets (quantum particles) through an adiabatic process [151,152]. For photons, the process results in the transformation of all the light from one edge to the other if the process is adiabatic, but disorder can cause some backscattering [153].

Due to the fact that this approach allows for demonstrating 2D physics with a magnetic field on a 1D lattice with just changing distances between sites, it was possible to experimentally observe, for the first time in photonics, topological pumping of edge states [55,61]. We will now explain how this was demonstrated experimentally in more detail. The experiment was done in a transparent dielectric medium with index of refraction $n_0 + \Delta n(\vec{r})$, where $\Delta n(\vec{r})$ represents small variations in the refractive index: $|\Delta n(\vec{r})| \ll n_0$. In this system, the light is propagating in the medium along the optical axis z, with the linearly polarized field $E(\vec{r}) = \psi(\vec{r}) e^{-ik_0 z} e^{i\omega t}$ (where $k_0 = \frac{\omega}{c} n_0$). We assume the paraxial approximation, which means that light only deviates by small angles from the optical axis: $|\frac{\partial \psi^2}{\partial z^2}| \ll 2k_0 |\frac{\partial \psi}{\partial z}|$. Substituting these expressions into the Helmholtz equation yields the following propagation equation, known as the paraxial wave equation:

$$i\frac{\partial\psi}{\partial z} = \frac{1}{2k_0}\nabla_\perp^2\psi + \frac{k_0}{n_0}\Delta n(\vec{r})\cdot\psi. \tag{8}$$

This equation is equivalent to the Schrodinger equation with two spatial dimensions, where the optical axis z plays the role of time, $\frac{k_0}{n_0}\Delta n(\vec{r})$ acts as the potential $V(\vec{r})$, and $\frac{1}{2k_0}\nabla_\perp^2$ is the kinetic term. To observe topological effects in this optical system, one can use a lattice potential $\Delta n(\vec{r})$, which is formed by an array of evanescently coupled waveguides. Thus, by fabricating a lattice with distances that correspond to the coupling in Eq. (4) [Fig. 3(a)], the wave dynamics is the same as the temporal evolution of a single electron in an AA lattice. Scanning ϕ (which is equivalent to the momentum in the synthetic space) is translated to scanning the 2D Brillouin zone with a 1D line. This scanning reveals the unidirectional evolution of edge states associated with the 2D Harper model system [Fig. 3(b)]. Thus, by adiabatically changing (in z) the coupling along the propagation axis (equivalent to adiabatically varying the hopping parameter in time), the photons are transferred ("pumped") between different regions of the topological band structure [Fig. 3(b)] and, consequently, move from one edge of the lattice to the other edge, through the bulk of the lattice [Fig. 3(c)].

The topological pumping (also known as Thouless pumping) is a phenomena that is not restricted to one type of topological lattice and also not to a single dimension. In fact, by extending this idea to a 2D physical lattice, which is the vector product of two 1D AA spatial lattices, one can obtain a representation of 4D quantum Hall physics, described by the Hamiltonian:

$$H = \sum\nolimits_{n,m} t_x c_{n,m}^\dagger c_{n+1,m} + t_y c_{n,m}^\dagger c_{n,m+1} + \text{h.c}, \tag{9}$$

where $t_i = \tilde{t}_i + \lambda_i\cos(2\pi b_i i + \phi_i)$, with $i = \{x, y\}$. In Eq. (9), each AA model is written in the off diagonal form [not in the diagonal form of Eq. (5)], but both of these representations map to the Harper model [55,61]. Here, ϕ_i represents two synthetic momenta in two different independent axes $\{k_z, k_w\}$, b_i represents the synthetic magnetic fields in two planes $x-z$ and $y-w$, and $\tilde{t}_i$, λ_i are constant parameters. Thus, the Hamiltonian has four quantum momentums—two real (k_x, k_y) and two synthetic—and it maps to four dimensions. Figure 4 shows a cross section scan of the 4D Brillion zone along the line $\phi_x = \phi_y$, which is equivalent to $k_z = k_w$. The 4D Hamiltonian has a first-order Chern number in each 2D plane, which accounts for the

Figure 3

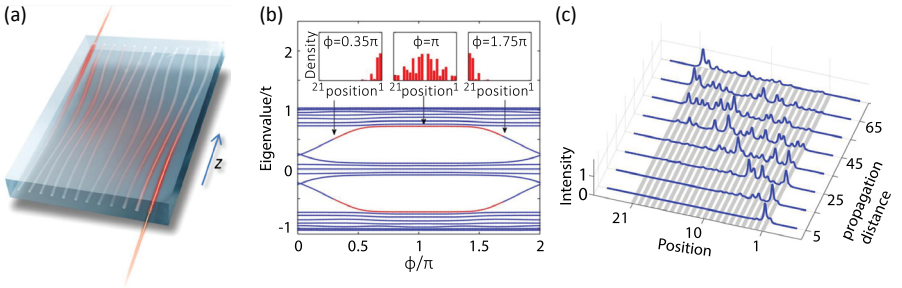

(a)–(c) 1D Andre–Aubry lattice exhibiting the physics of 2D integer quantum Hall effect [61]. (a) Illustration of the 1D waveguide array with adiabatically varying coupling along the propagation axis. Light is transferred ("pumped") from one edge to the other through the bulk of the lattice. (b) Band structure in parameter space, with ϕ being the index that changes adiabatically in the propagation axis z [61]. (c) Light transferred from edge to edge in the system described in (a) and (b).

multiple edge states in Fig. 4, but also a second-order Chern number in the 4D space, which corresponds to corner states. The explicit calculation of the 4D Chern number in the synthetic dimension is

$$C_j = -\frac{1}{8\pi^2}\int \varepsilon_{\mu\xi\rho\sigma}\, Tr\left[P_j \frac{\partial P_j}{\partial k_\mu}\frac{\partial P_j}{\partial k_\xi}\frac{\partial P_j}{\partial k_\rho}\frac{\partial P_j}{\partial k_\sigma}\right] d^4\boldsymbol{k}, \tag{10}$$

where $P_j(\boldsymbol{k})$ is the projector onto the subspace below gap j spanned by the extended Brillouin zone $\tilde{\boldsymbol{k}} = \{k_n, k_m, k_k, k_l\}$. The second Chern number (as the first Chern number) is related to quantized pumping and edge states.

In this fashion, even though the system describes a plane in the 4D hyper-volume at each moment, 4D topological pumping can be observed experimentally with a 2D paraxial photonic waveguide array [72,73] at each "instant" of the propagation along the propagation axis. The light has a 2D band structure, which is a 2D plane in the 4D band structure in parameter space. Consequently, by changing the coupling distances, it is possible to topologically pump light along a line in this 4D parameter space (Fig. 4).

This example is just one out of several experiments relying on synthetic dimensions in parameter space. In this vein, treating a static parameter as the quantum momentum was also used to experimentally demonstrate type-III Weyl semimetal [154], and other parameters (such as magnetic field) were used to show photonic Weyl points due to broken time-reversal symmetry [51] and exceptional surfaces [155]. While the experiment described above is based on a space that is a hybrid real-synthetic space, it is also possible to have a full synthetic parameter space. For example, it was demonstrated that specific inner layer parameters, p and q of a 1D photonic crystal, can form a 3D parameter space together with the wavenumber k. This parameter space has experimentally measurable Weyl points and edge states [75]. A similar approach was also used to observe exceptional cones in 4D parameter space [156].

To summarize, parametric synthetic dimensions represent a useful tool for demonstrating topological phases in high dimensions, with the main advantage being that, unlike other methods, here the complexity does not scale up with the dimensionality

Figure 4

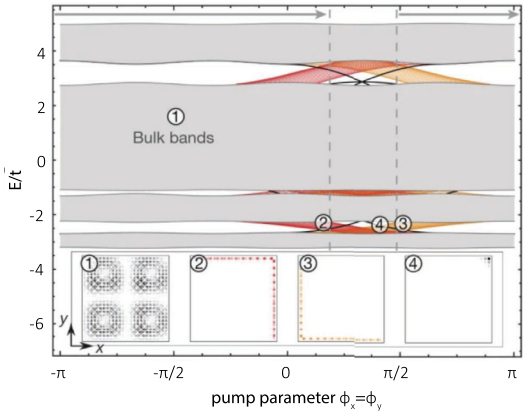

2D lattice exhibiting the physics of 4D integer quantum Hall effect [72]: eigenenergies of the system for $\phi_x = \phi_y$. The orange and red wedges in the dispersion curve are edge states (there are several due to different momentum in $k_x - k_y$). The black curves are corner states, which are not wedges in the dispersion curve.

of the topological phenomena as much as it does in other approaches. When a parameter represents a dimension, the additional experimental complexity is much smaller in this parametric method than when using the other methods for adding dimensionality [157]. On the other hand, a synthetic dimension lacking a kinetic term means that transport is fundamentally restricted to a lower dimensional subspace of the synthetic space. In the next section, we describe a different method for synthetic dimensions, in which all the dynamics is available at each instant and support transport in all dimensions, spatial and synthetic alike.

3.2 Synthetic Space Relying on Modal Ladders

In the previous method described above, the extension of dimensionality was based on a parameter that played the role of a synthetic dimension. Using a parameter p as the quantum momentum k implies that the Fourier transform space of p is the kinetic term $\frac{\partial}{\partial \tilde{p}}$, where $\tilde{p}$ is the "spatial" coordinate of the momentum p. However, static parameters stay constant under Fourier transform, which means that the Hamiltonian in synthetic space usually maps to a slice of a higher dimensional Hamiltonian.

On the other hand, if p—the synthetic dimension—is not a fixed parameter of the system but a quantity that can take different values depending on the wave function such as frequency, spin polarization, and momentum, then it can fully map to a spatial coordinate. The reason is that a wave can change these properties dynamically just as if it changes its location in space. Naturally, a wave does not change such quantities (as spin or energy) as it changes its location in space, so the technique we are about to describe focuses on engineering systems that make these quantities behave as spatial axes. For example, the quantity that we will now use to explain this concept is the energy of the wave function and, specifically, the energy ladder of a wave in a harmonic potential. We will now show how the dimensionality of an n-dimensional lattice of harmonic potentials can be increased by using the energy ladder of each harmonic potential. Furthermore, we will show how, by properly modulating the Hamiltonian in the time-domain, topological edge states emerge and the full dynamics of edge states in the high dimension can be observed.

For the sake of demonstration, we will use the Hamiltonian of a harmonic potential as in [81], but the principles apply to any kind of bounded potential for any wave (cavity, ring resonator, waveguide structure, etc.) [82–86,158,159]. Let us first look at a single potential well. The Hamiltonian for a harmonic potential can be obtained for photons by using quadratures, for example, for photons in a cavity or in waveguides with the paraxial equations, as will be shown in this review. The Hamiltonian for such harmonic potential is

$$H_0 = \frac{\hat{p}_x^2}{2M} + \frac{1}{2}M\omega^2\hat{x}^2 = \omega\sum_{E=0}^{\infty}\lambda|\lambda\rangle\langle\lambda|, \tag{11}$$

where $\hat{p}_x$ is the momentum operator in $\hat{x}$, M is a mass term, and ω is a fixed parameter. $|\lambda\rangle$ represents the equally spaced eigen-energies, which will be used for forming the synthetic dimension. For H_0, this ladder (1D lattice) of energies is completely decoupled. In order to couple the energies, we need to add external modulation:

$$\hat{H}_{\text{tot}} = \hat{H}_0 + \hat{V}(t) = \hat{H}_0 + \kappa\hat{x}\ \cos(\omega_D t + \phi), \tag{12}$$

where $\omega_D = \omega - \Delta$ with $\Delta \ll \omega$ and ϕ is a constant phase of the modulation. Now, the state basis $|\lambda\rangle$ is no longer an eigenbasis of H_{tot} since it is the eigenstate of the unperturbed Hamiltonian $\hat{H}_0$. However, we would still like to describe H_{tot} in the basis of $|\lambda\rangle$. The reason is that $|\lambda\rangle$ is our synthetic coordinate, and we deliberately couple the ladder of energies so that it will not be a "good" quantum number, but rather a wave

will travel along the λ coordinate as it travels in space, i.e., we would like H_{tot} to have a kinetic term. As in every basis change, the transition to the basis λ can be done by a unitary transformation. When transforming H_{tot} with $\hat{U} = \exp(it\omega_D\hat{\lambda})$ and using the rotating wave approximation, $\omega_D \gg \kappa\sqrt{\frac{\lambda}{8M\omega}}$, we obtain the following effective Hamiltonian:

$$H_{\text{eff}} = \Delta\sum_{\lambda}\lambda|\lambda\rangle\langle\lambda| + \sum_{\lambda}J_{\lambda}(|\lambda-1\rangle\langle\lambda|e^{i\phi} + \text{h.c}), \tag{13}$$

where J_λ is the effective coupling between modes and is equal to $J_\lambda = \kappa\sqrt{\frac{\lambda}{8M\omega}}$. The effective Hamiltonian obtained is that of a 1D lattice of modes [Fig. 5(a)] with an effective electric field Δ in the direction of the synthetic axis, and a phase term in the coupling: ϕ. At this stage, the effective electric field, which can be tuned by changing the size of Δ, affects the dynamics along the "modal dimension," but the phase ϕ does not since it can be gauged out. According to the gauge theory, a local phase degree of freedom of the wave function is equivalent to gauge fields (electric and magnetic fields) acting on the particles represented by the wave function—in our case, photons. At this point, the phase ϕ represents a global phase of the wave function and, thus, has no impact on the dynamics.

However, this will become completely different upon introducing more harmonic traps to the system, with a phase difference between one another. Having a phase $\phi(\vec{r})$ that depends on the location in space (of the harmonic trap) introduces a local gauge degree of freedom, which translates to gauge fields according the gauge theory. Indeed, by choosing different $\phi(\vec{r})$, it is possible to induce effective EM fields in the hybrid modal-spatial space. To see this in a simple form in our derivation, we couple such resonators with each other via proximity, in a spatial lattice with n dimensions. The coupling is resonant (hence, efficient) when phase matching is satisfied; that is, each mode is coupled to the same mode in its neighboring sites.

The idea is then to have an $n+1$ dimensional lattice, where the extra dimension is the ladder of modes associated with each site in the spatial lattice. Formally, this is achieved by a basis transformation of the Hamiltonian of the n-dimensional lattice of harmonic oscillators $H_{nD,\text{tot}}$ with the unitary transformation, $V = \otimes_s U$, which

Figure 5

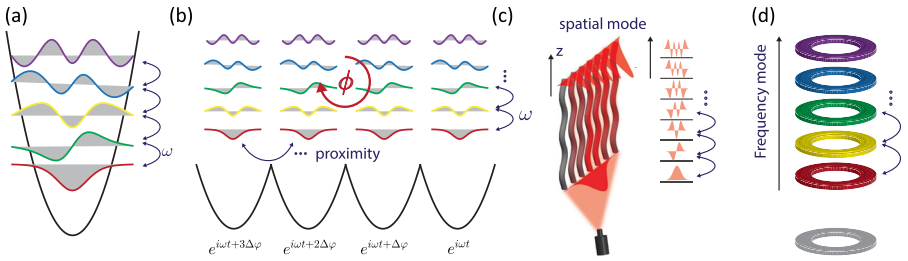

Mode ladder of a harmonic potential. The coupling between modes is achieved by modulation. (b) A 1D chain of equally spaced harmonic traps form a 2D synthetic space with one spatial dimension and one modal dimension. The modulation in each site couples the modal degree of freedom, and the phase difference results in magnetic flux. (c) and (d) Examples of realizations of the concept of using a ladder of modes as a synthetic dimension: (c) waveguide array structure with array modes coupled by oscillations in the propagation direction, thereby forming a synthetic dimension [85]; (d) an optical resonator that forms a ladder of modes coupled by temporal modulation, hence forming a synthetic dimension in frequency space.

is the tensor product of U with itself over the spatial dimension s. The resulting Hamiltonian is $H_{(n+1)D,\mathrm{eff}} = V^{\dagger} H_{nD,\mathrm{tot}} V$.

This recipe, which can be applied to any kind of arrangement of sites with inner modes, results in the following Hamiltonian for an $n+1$ dimensional lattice:

$$H_{(n+1)D,\mathrm{eff}} = \Delta_s \sum_{\lambda,s} \lambda |\lambda, s\rangle\langle\lambda, s| + J_\lambda (|\lambda - 1, s\rangle\langle\lambda, s| e^{i\phi_s} + \mathrm{h.c}) + J_{s,\lambda} (|\lambda, s-1\rangle\langle\lambda, s| + \mathrm{h.c}), \tag{14}$$

where $J_{s,\lambda}$ is the spatial coupling between mode λ in sites s and $s-1$, and is dependent on the geometry of the lattice, and ϕ_s, Δ_s are the phase term ϕ and frequency bias term Δ, which are dependent on the modulation phase and frequency at each site s. Importantly ϕ_s, Δ_s form effective gauge fields (magnetic and electric) in the synthetic dimension, which can be controlled by adjusting a different modulation in each site. For example, a 1D system $s = \{1, \ldots m\}$, with $\phi_s = s\frac{\pi}{2}\phi$ and $\Delta_s = 0$, corresponds to a 2D lattice with a perpendicular magnetic field with flux $\pi/2$ in each unit cell, and 0 electric field since $\Delta_s = 0$ [Fig. 5(b)]. With these parameters, Eq. (14) becomes the Hamiltonian of the IQH, which is a 2D model that is now realized on a 1D spatial lattice. This idea was demonstrated experimentally in two different platforms in photonics (spatial modes of an array of waveguides and frequency modes of a temporally modulated ring resonator [85,88]), in microwaves [86] and also, before that, in cold atoms with spin modes [76,77] and momentum modes [79].

We will now explain how this was realized in photonics and what the implications are of such realizations on physical photonic systems. We go back to the physical system of light propagating in a paraxial waveguide array (as discussed in Section 3.1). In order to have synthetic dimensions in modal space, the first step is to have a confined structure with a ladder of modes [examples in Figs. 5(c) and 5(d)]. This confined structure plays the role of the harmonic trap as in the example above. In direct analogy to the harmonic trap example, it is possible to create a harmonic potential by changing the index refraction $\Delta\varepsilon(\vec{r})$ in a dielectric material. Conveniently, instead of encoding a continuous harmonic potential in the permeability $\Delta\varepsilon(\vec{r})$, it is possible to have a potential made of discrete (single-mode) waveguides at varying distances, so as to obtain the equally spaced modal structure of a harmonic potential. This lattice is called a J_x lattice, and in this lattice the distances between adjacent waveguides increase as a function of their distance from the lattice center [Fig. 6(a)] [160]. As a harmonic potential, the J_x lattice has equally spaced modes that function as the synthetic space. In order to couple the modes, an external perturbation is needed [Eq. (12)]. The perturbation itself can take many forms. One option is to oscillate the waveguide spatially at exactly the longitudinal spatial frequency that separates the different modes [Fig. 6(b)]. Thus, this J_x structure of a waveguide lattice functions as a harmonic trap, and it can be placed near other identical J_x lattices and obtain a Hamiltonian as in Eq. (14). For example, placing the J_x lattices near each other in a row such that they are evanescently coupled [Fig. 6(c)] corresponds to a 2D synthetic space with two dimensions: one spatial dimension (the location of the J_x lattice along x axis) and one synthetic dimension (the mode of each J_x lattice). In the 1D row of different J_x lattices, each J_x lattice oscillates at a different phase according to $\phi_s = s\frac{\pi}{2}\phi$, where s counts the J_x lattice along the x axis. A phase shift in ϕ_s that breaks the z-reversal symmetry in the paraxial equation is equivalent to an effective magnetic field [see Eq. (14)] and induces the formation of edge states in the synthetic space lattice. Importantly, just as for the Harmonic traps, it is possible also to place the J_x photonic topological insulators in a geometry of a 2D lattice (for example, a diamond lattice) and obtain lattices in three dimensions [85,161] with a 2D lattice geometry.

To understand the dynamics of the propagation of light on the edge of a space with one spatial dimension and one synthetic dimension, we describe a wave packet that propagates along the edge state in synthetic dimension of the waveguide structure described.

In practice, the direct meaning of this in photonics is that we can design photonic systems with a topologically protected transport that is not on the spatial edge of the lattice. Rather, the protected transport can be in the bulk of the lattice instead of the edge [85], in the frequency dimension [84,88], or in both dimensions simultaneously—for example, in a spiral motion [89]. To understand what it means, let us analyze the propagation of light in an edge state in the modal dimension, as illustrated by Fig. 6(c).

A single edge state in the synthetic space of Fig. 6 encircles the perimeter of the 2D synthetic structure shown in Fig. 6(c). Thus, a wave packet propagating along the edge in this synthetic space comprises a superposition of edge states and takes the following course. In Stage A in Fig. 6(c), the wave packet propagates to the left in the lowest mode of each J_x lattice; a snapshot of the propagating wave packet in real space is given in Fig. 6(d). Note that the lowest mode is the edge in synthetic space, but not the edge in real space, as seen in Fig. 6(d). In fact, at this point the synthetic space edge state is extended on the entire real-space lattice. This, however, does not change the fact that its transport is topologically protected [162], since the edge state is still a state crossing the gap exactly as an edge state in the IQH [see Fig. 1(c)]. When this state reaches the leftmost J_x lattice of the array, it does not scatter backward but

Figure 6

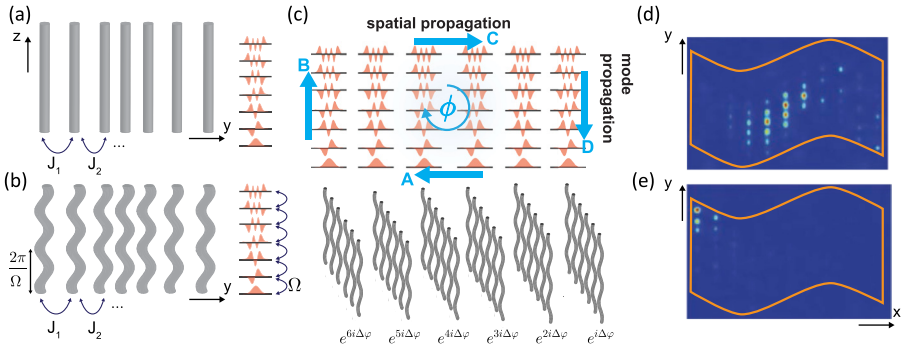

(a) J_x waveguide array with equally spaced spatial modes. The modes are separated by a longitudinal spatial frequency Ω. (b) The same J_x lattice as in (a), but here it oscillates in z, at a frequency equal to Ω. The oscillation couples the modes, thereby creating a 1D lattice in synthetic space. A wavepacket initially populating the lowest mode is efficiently transferred to the second mode by the modulation, then to the third mode, etc. (c) A row of J_x lattices (columns) and above it the 2D picture in synthetic dimensions, where the horizontal axis is the location of every J_x lattice (column) and the vertical axis is the mode in each J_x lattice. The arrows indicate the directionality of the topological edge state in the synthetic dimension. (d) and (e) The real-space intensity of the light when propagating in the structure: (d) is on the bottom edge [see A in (c)], so the wavepacket populates a single lower mode (extended) on many J_x lattices. (e) The wavepacket at instant B in the propagation—on the leftmost edge. In this case, the light is in a coherent superposition of modes on the leftmost J_x lattice (concentrated due to interference between the modes). The frame of the lattice has a wave shape since the columns oscillate at a different phase along the vertical real-space dimension (adapted from [85]).

rather concentrates entirely on the leftmost J_x and starts ascending in the modes unidirectionally (Stage B). At this point, the wave packet is in a superposition of modes that appears as a concentrated wave packet [Fig. 6(e)]. After ascending to the top mode, the light propagates to the right, while remaining strictly in the top mode at Stage C. Finally, the light descends to the lowest mode on the rightmost J_x lattice. In doing that, the wave packet has completed a full cycle of transport around the synthetic space edge.

As mentioned earlier, robust topological propagation in non-spatial dimensions is by itself interesting even before considering the dimensionality increase. In these systems, the light performs a robust unidirectional ascent (or descent) on the modal ladder, which can potentially be used in future applications. One example of a potential application of synthetic space systems relying on modal ladders is the recent proposal for a mode-locked topological insulator laser [93]. In short, a topological insulator laser is an array of emitters (typically semiconductor lasers) judiciously positioned on a topological photonic platform, so as to force locking of all the emitters associated with the topological mode, making them act as a single high-power coherent laser source [41,93,139,140,163–167].

The topological photonic platform can be any of the 2D platforms described above, where each site is replaced by a laser emitter (e.g., a microring laser), with pumping provided preferentially to the edge mode. What makes the emitters lock together is two features of topological edge modes: (1) the non-zero velocity, implying that the light in the edge mode must travel between all emitters associated with the edge mode and (2) the topological robustness, which facilitates coupling between emitters despite some inevitable level of imperfections or disorder. Thus far, however, all the settings in which topological insulator lasers were demonstrated were real-space topological platforms, and they were geared toward coherent locking of many emitters to a single frequency. But a recent proposal has targeted a different goal: locking many emitters in a train of equally spaced frequencies for the purpose of generating mode-locked laser pulses from a large array of semiconductor lasers [93]. The necessity of locking a train of frequencies naturally suggested the use of synthetic dimensions, with the frequency eigenmodes of the laser resonators acting as the modal dimension.

Let us describe that system in some detail. Considering a row of coupled ring resonators [83,84], we can treat each ring resonator in the same way we did with the harmonic trap. The ring resonator also has a ladder of equally spaced resonance frequencies that can be coupled by electro-optic phase modulation [Fig. 7(a)]. This turns each ring resonator into a 1D lattice of modes. Then, as before, a row of ring resonators represents a 2D lattice with one spatial dimension—the location of each ring—and one synthetic dimension—the frequency mode of each ring. This principle was recently demonstrated on a single ring with two ladders (each frequency is actually degenerate to two modes—clockwise and anticlockwise), and it was shown experimentally that this structure can have synthetic magnetic fields [88] and even exhibit non-Hermitian physics [168]. Each ring can be made to lase by adding saturable gain, and together with the electro-optical modulation a ring laser can be made to mode-lock and emit a train of mode-locked pulses. However, if we would like several such rings to mode-lock together, it is virtually impossible to synchronize all the ring resonators to lock on the same train of equally spaced frequencies. This is simply because coupling just two rings causes the splitting of each mode, resulting in two sets of equally spaced frequencies. In this vein, having N rings creates N sets of frequencies, and it becomes virtually impossible to get all rings to synchronize on the same set of frequencies, as required for coherent emission of mode-locked pulses. In fact, the largest number of semiconductor emitters that was ever made to mutually

mode-lock is 10 [169]. Here is where the concept of topology in synthetic dimensions gets into play. If the lasing mode is an edge state engulfing several rings, it may force them to mode-lock together without dephasing due to the topological protection. Such structure was suggested in [93] and has an elaborated pattern for the gain in each ring [Fig. 7(b)].

Another avenue where synthetic dimensions can have a large impact is in the world of nonlinear optic systems [81,170,171]. Since experimentally studying interacting systems in dimensions higher than three is physically impossible (at least for the time being), facilitating the ability to do so in synthetic space photonics can have major impact on fundamental issues. Nonlinear physics in high dimensions is one of those fields [170,172]. As a pioneering example, in [170], it was proposed to have ring resonators with $\chi^{(3)}$ nonlinearity and modulated group velocity dispersion (GVD) [Fig. 7(c)]. In this case, the $\chi^{(3)}$ nonlinearity maps to local interactions in synthetic space, allowing to simulate interacting quantum many-body systems resembling the local interactions of electronic condensed matter systems.

The experimental demonstration of nonlinear frequency conversion to produce high-dimensional physics with gauge fields in nonlinear waveguides is another promising realization of the modal dimension experimental approach [173], and quantum interactions of photons on nonlinear frequency combs were also suggested in the context of four wave mixing [171].

Other suggestions for utilizing the modal dimension approach focus on extending the dimensionality of topological systems. Some of these suggestions were never demonstrated experimentally in any system. As mentioned, by using both the extra lattice dimension [83] and the long-range coupling [174,175] in the modal dimension approach in the linear and nonlinear regimes, it is possible to experimentally study high-dimensional topological phases and topological phases that are hard to realize in ordinary lattices. Several suggestions for models, such as 3D Weyl points [90], 3D PT symmetric models [53], Haldane model [175]. Likewise, high-order topological insulators [91], evolution invariant synthetic space topological insulators [98], and more, are waiting to be realized experimentally with the modal dimensions approach.

3.3 Using Time-Bins as Synthetic Dimension

In the previous approaches, the synthetic dimension was either a parameter of the Hamiltonian (such as the coupling strength) or a variable of the wave function such as spin or frequency, which were exploited for generating a modal ladder acting as a

Figure 7

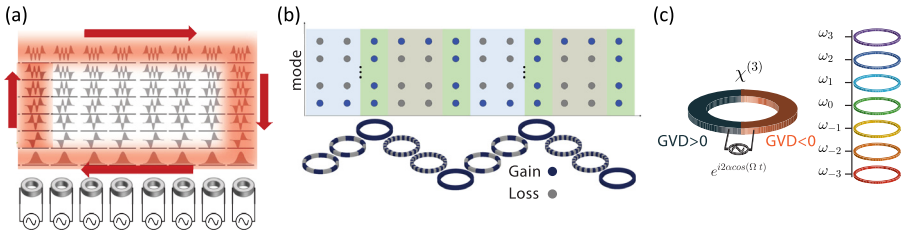

(a) Edge state in the synthetic modal space of a row of phase modulated ring resonators. (b) A chain of modulated ring resonators with selective saturable gain that forms an edge state. This causes a topological edge state to lase given robust properties to the lasing (adapted from [93]). (c) Temporally modulated ring resonator with χ^3 nonlinearity and spatially modulated GVD can support Hamiltonians with local interactions in synthetic space (adapted from [170]).

synthetic dimension. In the third approach, the synthetic dimension is a coordinate—specifically, the only coordinate that is not spatial: time. However, time usually already has a role in topological systems—it is the evolution parameter. Hence, if time were to be used as a synthetic dimension, it would be necessary to somehow exchange between time and space [176]. But how can this be used to increase dimensionality?

A popular method to do just that is by time-bin encoding. To understand this concept, consider an arbitrary wave function ψ_0 in N dimensions that undergoes a periodic modulation every time period T. The evolution of ψ_0 after time T can be described by the unitary operation U, which satisfies $\psi_{nT} = U^n \psi_0$, where n is the number of periods that the wave function went through. The operator U corresponds to an effective Floquet Hamiltonian according to

$$U^n = e^{-iH_{\text{eff}}nT}, \tag{15}$$

where H_{eff} is a static effective Hamiltonian. Notice that the full temporal dynamics of H_{eff} coincide with the dynamics ψ_{nT} at the beginning of each period. The Floquet Hamiltonian is known to exhibit topological phases in a variety of lattice systems [25,29,177], but here we will not assume any underlying spatial lattice whatsoever. Since analyzing the dynamics of this system requires sampling it every period T, the remaining time on the time axis remains unused. The idea then is to utilize the "unused time" as a spatial degree of freedom. If each time-bin represents a different location in space, adding a delay Δt $(-\Delta t)$ to the information expected to arrive at time nT means that the information has moved one step to the right (or left).

On the basis of the time-bin lattice with an additional degree of freedom of the Hamiltonian (such as polarization), it is possible to construct a system with a topological band structure, where the Brillouin zone is the reciprocal space to the time-bins, and the additional degree of freedom allows for the complexity required for the non-trivial topology. To understand this, consider a typical system composed of two coupled fiber loops with different length $x \pm \Delta x$, as shown in Fig. 8(a). A light pulse is launched into the system and completes encircling each fiber in times $T \pm \Delta T$, depending on which fiber it travels in. After completing n periods, the pulse can be in one of the following times: $t = nT + p\Delta T$, $p = \{-n, -n+1, \ldots, n\}$. Thus, each value of p is a time-bin, and it is a synthetic dimension that represents a location in space. Each time ΔT is regarded as one step in the motion in which the photon can move left or right in this synthetic space [Fig. 8(b)]. In principle, additional synthetic space dimensions can be obtained by using several time scales. That is, adding another bin splitting to obtain two different paths with temporal difference $\Delta \tilde{T}$, which is larger than $2n\Delta T$, makes it possible to have another synthetic spatial dimension. The pulses in the system have a spatial dimensionality of the number of time scales added, but in order to have a sense of a geometric phase involved in topological phases, another degree of freedom is added to the spatial one. In the system described in Fig. 8, it is the polarization of the pulse. The polarization is described by a 2D vector and can accumulate a phase and, thus, a geometric phase. In this setting, topological edge states can be obtained by coupling the polarization degree of freedom to the translation degree of freedom. This operation can be done simply by using a polarization-dependent beam splitter, which can be described by the following operator:

$$T_x = \sum\nolimits_x |x+1\rangle\langle x| \otimes |\uparrow\rangle\langle\uparrow| + |x-1x\rangle\langle| \otimes |\downarrow\rangle\langle\downarrow|\,, \tag{16}$$

where $|x\rangle$ is the synthetic position degree of freedom and $|\uparrow\rangle$ $(|\downarrow\rangle)$ is the spin up (down). The polarization here is analogous to the geometric phase of the wave function, which is responsible for the topological effects described in previous sections.

To obtain a topological phase in 1D, we split T_x to two operators, $T_\uparrow$ ($T_\downarrow$), which move the light one site right (left) if the spin is up (down). Then, by adding two rotations between the two splitted parts of T_x we obtain

$$U_{1D} = T_\uparrow R(\theta_2) T_\downarrow R(\theta_1), \tag{17}$$

where $R(\theta)$ is polarization rotation by angle θ. The DTQW related to this operator [Fig. 8(c)] has a topological phase diagram with two possible topological phases [Fig. 8(d)]. The topological phases are characterized by the Zak phase from Eq. (1) of the effective Hamiltonian [178]. The implication of a boundary in the DTQW between different regions with different θ_2 [Fig. 8(e)], and with different topological phases, can be seen in the left panel [Fig. 8(f)]. Exciting the edge state causes localization, where the wave remains concentrated on the edge without coupling to neighboring sites. This is contrary to the right panel in which the two regions have the same topological phase (but different θ_2), and in this case no localization occurs. As for the system described in previous sections, the studies on these synthetic dimensions can be extended both in dimensionality and in fundamental properties such as hermiticity and nonlinearity. Moreover, by considering an additional time scale—it is possible to add the same spin dependence also in y: T_y and to consider the cyclic process:

Figure 8

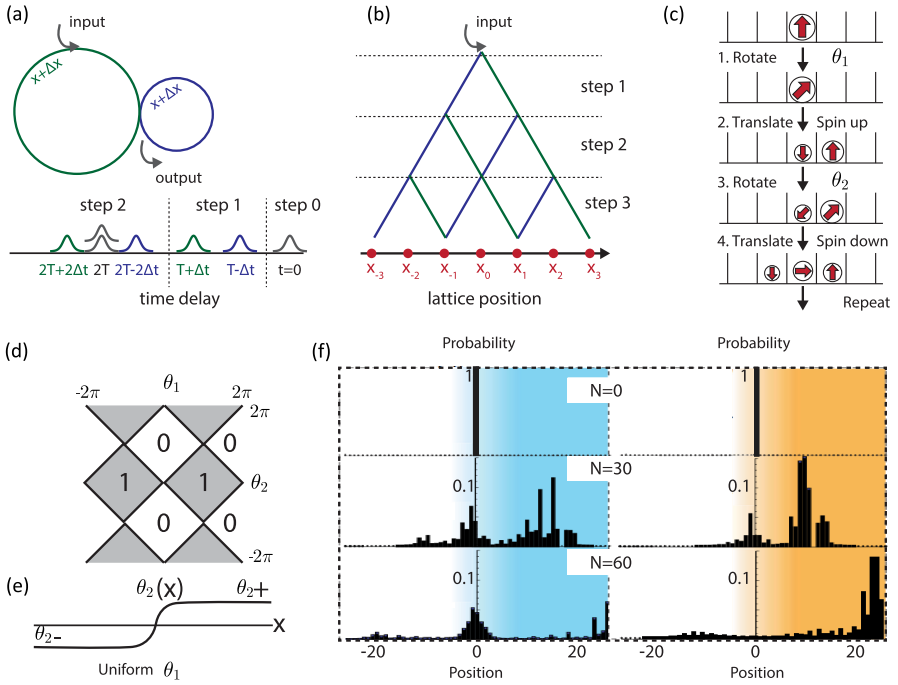

(a) Illustration of two coupled fiber loops of different lengths. Different output arrival times correspond to different locations on a 1D lattice in space. (b) Steps of the discrete time quantum walks (DTQWs) corresponding to the two-fiber setting in (a) (adapted from [179]). (c) DTQW coupling of the polarization degree of freedom to the spatial (time-bins) degree of freedom in a DTQW process [113]. (d) Topological phase diagram corresponding to different rotation angles θ_1 and θ_2 of the process in (c). Here, gray regions correspond to non-trivial topology with Rudner number 1 [113]. (e) A boundary with edge states forming by changing θ_2 [113]. (f) Edge propagation of two regions in the DTQW. In the left panel, the two regions are in a different topological phase inducing a localized state on the edge. In the right panel, the two regions have distinct θ_2 but same topological phase, so no localization occurs [113].

$$U = T_y R(\theta_2) T_x R(\theta_1). \tag{18}$$

The process described by this equation also has topological phases, and, since it is a 2D model, the topological properties are different from those of the 1D model. In this Floquet system, the topological invariant is the Rudner number [180]. Just like the Chern number, the Rudner number predicts the existence of unidirectional robust edge states in the gap. As in the 1D case, one can have a phase diagram as of a function of θ_1 and θ_2 [Fig. 9(a)]. The edge state at the boundary between different values of θ_1 is illustrated in Fig. 9(b), and the band diagram. The reason that the Chern number is not used here is because the Chern number gives for each band the difference between the number of edge states bellow the band and above the band. Since in this type of Floquet Hamiltonians the difference is zero (but edge states still exist) [see Figs. 9(c) and 9(d)], the Rudner number, which takes into account the temporal dependence of the Hamiltonian, is the proper quantity to use.

The propagation of light in this system is simulated in Fig. 9(e). The light bypasses two corners along the edge, demonstrating the topological robustness of the propagation [125].

Figure 9

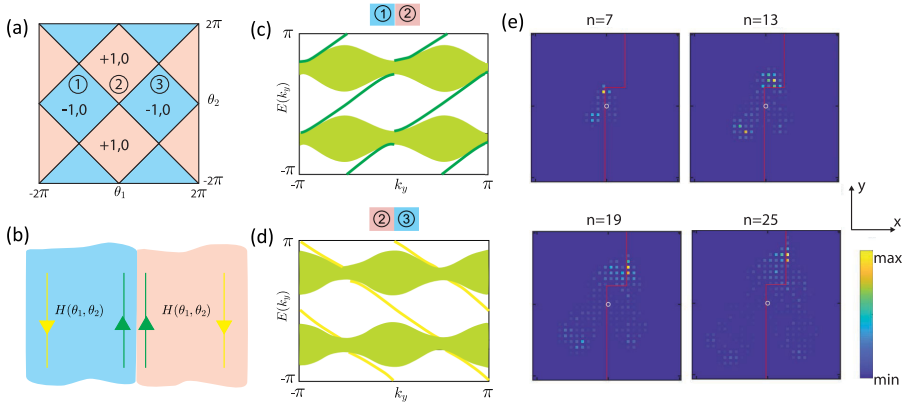

(a)–(e) 2D topology in DTQW [125]. (a) Topological phase diagram of the 2D DTQW for different values of θ_1 and θ_2. Each color corresponds to a different Rudner number. (b) Illustration of the unidirectional edge state propagation in the spatial synthetic space. (c) and (d) Band structure with edge states for different boundaries. (e) Propagation around an edge with two corners at different stages in the evolution.

Figure 10

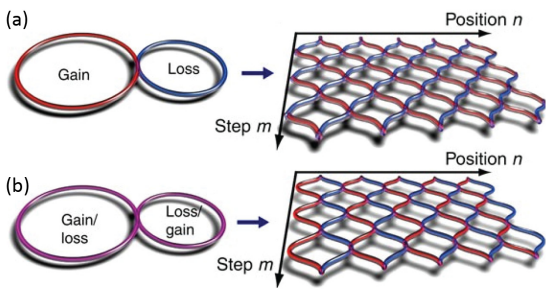

(a) Non-Hermitian fiber loop setup. (b) PT-symmetric fiber loop setup. The purple color on the fiber loops indicates that the gain and loss are alternating on every other round trip [111].

As in previous approaches discussed, beyond extending the dimensionality of the models, it is also possible to study non-Hermitian Hamiltonians with the DTQW. This can be done by adding gain and loss to the fibers [Fig. 10(a)], and, if added in an alternating fashion, it can also simulate a PT-symmetric lattice [Fig. 10(b)] [59]. Furthermore, in recent works, even solitons [111] and synthetic gauge fields [124] were studied, which shows the wide possibilities of these systems in studying novel physics using synthetic dimensions.

4. FUTURE DIRECTIONS AND VISION

In this review, we explained the basic physics of topological phases in synthetic dimensions and described the three different approaches for using synthetic dimensions in photonics, supporting topological phases and topological edge states. All of these approaches have already demonstrated the important experimental milestone of having 2D topological phases and topological edge states. These efforts are important for establishing this field experimentally, but we are now entering the most exciting stage of this field: experimentally studying topological phases that were never observed in any other experimental platform, whether if they are with high dimensionality, non-linear or non-Hermitian. Naturally, this is the most exciting stage, where synthetic dimensions can present opportunities where no one has gone before. As has already happened with "ordinary" photonic topological insulators based on spatial lattices, utilizing synthetic dimensions in experiments can lead to new theoretical and technological ideas, which are already starting to appear. The paradigm of robust control over the evolution of photons in synthetic dimensions offers new possibilities, as the propagation is no longer confined to spatial edges of the system. Another avenue where exciting research lies ahead is in simulating quantum interacting many-body models. Such models in high dimensions, with or without non-Hermiticity, are of fundamental value, and photonics presents an unprecedented opportunity to study them in the lab.

FUNDING

Air Force Office of Scientific Research; Israel Science Foundation.

ACKNOWLEDGMENT

Eran Lustig is supported by the Adams Fellowship Program of the Israel Academy of Sciences and Humanities.

DISCLOSURES

The authors declare no conflicts of interest.

REFERENCES AND NOTES

1. C. L. Kane and E. J. Mele, "Quantum spin Hall effect in graphene," Phys. Rev. Lett. **95**, 226801 (2005).
2. B. A. Bernevig, T. L. Hughes, and S.-C. Zhang, "Quantum spin Hall effect and topological phase transition in HgTe quantum wells," Science **314**, 1757–1761 (2006).
3. M. König, S. Wiedmann, C. Brüne, A. Roth, H. Buhmann, L. W. Molenkamp, X.-L. Qi, and S.-C. Zhang, "Quantum spin Hall insulator state in HgTe quantum wells," Science **318**, 766–770 (2007).

4. D. Hsieh, D. Qian, L. Wray, Y. Xia, Y. S. Hor, R. J. Cava, and M. Z. Hasan, "A topological Dirac insulator in a quantum spin Hall phase," Nature **452**, 970–974 (2008).
5. H. Lin, L. A. Wray, Y. Xia, S. Xu, S. Jia, R. J. Cava, A. Bansil, and M. Z. Hasan, "Half-Heusler ternary compounds as new multifunctional experimental platforms for topological quantum phenomena," Nat. Mater. **9**, 546–549 (2010).
6. D. Thouless, M. Kohmoto, M. Nightingale, and M. den Nijs, "Quantized Hall conductance in a two-dimensional periodic potential," Phys. Rev. Lett. **49**, 405–408 (1982).
7. K. V. Klitzing, G. Dorda, and M. Pepper, "New method for high-accuracy determination of the fine-structure constant based on quantized Hall resistance," Phys. Rev. Lett. **45**, 494–497 (1980).
8. B. I. Halperin, "Quantized Hall conductance, current-carrying edge states, and the existence of extended states in a two-dimensional disordered potential," Phys. Rev. B **25**, 2185–2190 (1982).
9. A. H. MacDonald and P. Středa, "Quantized Hall effect and edge currents," Phys. Rev. B **29**, 1616–1619 (1984).
10. Y. Hatsugai, "Chern number and edge states in the integer quantum Hall effect," Phys. Rev. Lett. **71**, 3697–3700 (1993).
11. F. D. M. Haldane, "Model for a quantum Hall effect without Landau levels: condensed-matter realization of the 'parity anomaly'," Phys. Rev. Lett. **61**, 2015–2018 (1988).
12. L. Fu, C. L. Kane, and E. J. Mele, "Topological insulators in three dimensions," Phys. Rev. Lett. **98**, 106803 (2007).
13. J. E. Moore and L. Balents, "Topological invariants of time-reversal-invariant band structures," Phys. Rev. B **75**, 121306 (2007).
14. A. Y. Kitaev, "Fault-tolerant quantum computation by anyons," Ann. Phys. (N. Y.) **303**, 2–30 (2003).
15. A. R. Mellnik, J. S. Lee, A. Richardella, J. L. Grab, P. J. Mintun, M. H. Fischer, A. Vaezi, A. Manchon, E.-A. Kim, N. Samarth, and D. C. Ralph, "Spin-transfer torque generated by a topological insulator," Nature **511**, 449–451 (2014).
16. Magnetic disorder breaks this topological protection.
17. M. Z. Hasan and C. L. Kane, "Colloquium: topological insulators," Rev. Mod. Phys. **82**, 3045–3067 (2010).
18. Topological insulators are not restricted to classical wave physics only. Rather, there are examples of topological insulators that fundamentally rely on interactions such as the fractional quantum Hall systems. However, the fundamental concepts of topological insulators do not require quantum interactions: they rely on wave phenomena such as interference and geometrical phases.
19. F. D. M. Haldane and S. Raghu, "Possible realization of directional optical waveguides in photonic crystals with broken time-reversal symmetry," Phys. Rev. Lett. **100**, 013904 (2008).
20. Z. Wang, Y. D. Chong, J. D. Joannopoulos, and M. Soljačić, "Reflection-free one-way edge modes in a gyromagnetic photonic crystal," Phys. Rev. Lett. **100**, 013905 (2008).
21. Z. Wang, Y. Chong, J. D. Joannopoulos, and M. Soljačić, "Observation of unidirectional backscattering-immune topological electromagnetic states," Nature **461**, 772–775 (2009).
22. R. O. Umucalılar and I. Carusotto, "Artificial gauge field for photons in coupled cavity arrays," Phys. Rev. A **84**, 043804 (2011).
23. M. Hafezi, E. A. Demler, M. D. Lukin, and J. M. Taylor, "Robust optical delay lines with topological protection," Nat. Phys. **7**, 907–912 (2011).

24. A. B. Khanikaev, S. H. Mousavi, W.-K. Tse, M. Kargarian, A. H. MacDonald, and G. Shvets, "Photonic topological insulators," Nat. Mater. **12**, 233–239 (2012).
25. M. C. Rechtsman, J. M. Zeuner, Y. Plotnik, Y. Lumer, D. Podolsky, F. Dreisow, S. Nolte, M. Segev, and A. Szameit, "Photonic Floquet topological insulators," Nature **496**, 196–200 (2013).
26. M. Hafezi, S. Mittal, J. Fan, A. Migdall, and J. M. Taylor, "Imaging topological edge states in silicon photonics," Nat. Photonics **7**, 1001–1005 (2013).
27. S. Mittal, J. Fan, S. Faez, A. Migdall, J. M. Taylor, and M. Hafezi, "Topologically robust transport of photons in a synthetic gauge field," Phys. Rev. Lett. **113**, 087403 (2014).
28. W.-J. Chen, S.-J. Jiang, X.-D. Chen, B. Zhu, L. Zhou, J.-W. Dong, and C. T. Chan, "Experimental realization of photonic topological insulator in a uniaxial metacrystal waveguide," Nat. Commun. **5**, 5782 (2014).
29. G. Q. Liang and Y. D. Chong, "Optical resonator analog of a two-dimensional topological insulator," Phys. Rev. Lett. **110**, 203904 (2013).
30. J. Nichols, X. Gao, S. Lee, T. L. Meyer, J. W. Freeland, V. Lauter, D. Yi, J. Liu, D. Haskel, J. R. Petrie, E.-J. Guo, A. Herklotz, D. Lee, T. Z. Ward, G. Eres, M. R. Fitzsimmons, and H. N. Lee, "Emerging magnetism and anomalous Hall effect in iridate–manganite heterostructures," Nat. Commun. **7**, 12721 (2016).
31. L. J. Maczewsky, J. M. Zeuner, S. Nolte, and A. Szameit, "Observation of photonic anomalous Floquet topological insulators," Nat. Commun. **8**, 13756 (2017).
32. L.-H. Wu and X. Hu, "Scheme for achieving a topological photonic crystal by using dielectric material," Phys. Rev. Lett. **114**, 223901 (2015).
33. S. Yves, R. Fleury, T. Berthelot, M. Fink, F. Lemoult, and G. Lerosey, "Crystalline metamaterials for topological properties at subwavelength scales," Nat. Commun. **8**, 16023 (2017).
34. Y. Yang, Y. F. Xu, T. Xu, H.-X. Wang, J.-H. Jiang, X. Hu, and Z. H. Hang, "Visualization of a unidirectional electromagnetic waveguide using topological photonic crystals made of dielectric materials," Phys. Rev. Lett. **120**, 217401 (2018).
35. M. A. Gorlach, X. Ni, D. A. Smirnova, D. Korobkin, D. Zhirihin, A. P. Slobozhanyuk, P. A. Belov, A. Alù, and A. B. Khanikaev, "Far-field probing of leaky topological states in all-dielectric metasurfaces," Nat. Commun. **9**, 909 (2018).
36. S. Barik, A. Karasahin, C. Flower, T. Cai, H. Miyake, W. DeGottardi, M. Hafezi, and E. Waks, "A topological quantum optics interface," Science **359**, 666–668 (2018).
37. T. Ma and G. Shvets, "All-Si valley-Hall photonic topological insulator," New J. Phys. **18**, 25012 (2016).
38. Y. Kang, X. Ni, X. Cheng, A. B. Khanikaev, and A. Z. Genack, "Pseudo-spin–valley coupled edge states in a photonic topological insulator," Nat. Commun. **9**, 3029 (2018).
39. M. I. Shalaev, W. Walasik, A. Tsukernik, Y. Xu, and N. M. Litchinitser, "Robust topologically protected transport in photonic crystals at telecommunication wavelengths," Nat. Nanotechnol. **14**, 31–34 (2019).
40. T. Ozawa, H. M. Price, A. Amo, N. Goldman, M. Hafezi, L. Lu, M. C. Rechtsman, D. Schuster, J. Simon, O. Zilberberg, and I. Carusotto, "Topological photonics," Rev. Mod. Phys. **91**, 015006 (2019).
41. M. Segev and M. A. Bandres, "Topological photonics: where do we go from here?" Nanophotonics **10**, 425–434 (2020).

42. A. B. Khanikaev and G. Shvets, "Two-dimensional topological photonics," Nat. Photonics **11**, 763–773 (2017).
43. X.-C. Sun, C. He, X.-P. Liu, M.-H. Lu, S.-N. Zhu, and Y.-F. Chen, "Two-dimensional topological photonic systems," Prog. Quantum Electron. **55**, 52–73 (2017).
44. There is also considerable literature on 1D topological photonic systems, mostly relying on the 1D binary lattice known as the SSH model [N. Malkova, I. Hromada, X. Wang, G. Bryant, and Z. Chen, "Observation of optical Shockley-like surface states in photonic superlattices," Opt. Lett. **34**, 1633–1635 (2009)]. These 1D systems are endowed with zero-dimensional edge states, but because their low dimensionality are not topological insulators, they are therefore generally not discussed in this review.
45. A. Kitaev, "Periodic table for topological insulators and superconductors," AIP Conf. Proc. **1134**, 22–30 (2009).
46. Z. Gong, Y. Ashida, K. Kawabata, K. Takasan, S. Higashikawa, and M. Ueda, "Topological phases of non-Hermitian systems," Phys. Rev. X **8**, 031079 (2018).
47. B. Lian and S.-C. Zhang, "Weyl semimetal and topological phase transition in five dimensions," Phys. Rev. B **95**, 235106 (2017).
48. X.-L. Qi, T. L. Hughes, and S.-C. Zhang, "Topological field theory of time-reversal invariant insulators," Phys. Rev. B **78**, 195424 (2008).
49. B. Lian and S.-C. Zhang, "Five-dimensional generalization of the topological Weyl semimetal," Phys. Rev. B **94**, 041105 (2016).
50. L. Lu, Z. Wang, D. Ye, L. Ran, L. Fu, J. D. Joannopoulos, and M. Soljačić, "Experimental observation of Weyl points," Science **349**, 622–624 (2015).
51. D. Wang, B. Yang, W. Gao, H. Jia, Q. Yang, X. Chen, M. Wei, C. Liu, M. Navarro-Cía, J. Han, W. Zhang, and S. Zhang, "Photonic Weyl points due to broken time-reversal symmetry in magnetized semiconductor," Nat. Phys. **15**, 1150–1155 (2019).
52. J. Noh, S. Huang, D. Leykem, Y. D. Chong, K. P. Chen, and M. C. Rechtsman, "Experimental observation of optical Weyl points and Fermi arc-like surface states," Nat. Phys. **13**, 611–617 (2017).
53. E. Lustig, Y. Plotnik, Z. Yang, and M. Segev, "3D parity time symmetry in 2D photonic lattices utilizing artificial gauge fields in synthetic dimensions," in *Conference on Lasers and Electro-Optics, OSA Technical Digest* (Optical Society of Ameria, 2019), paper FTu4B.1.
54. Note that, beyond periodic systems, topological phases (without topologically protected edge transport) in 1D quasicrystals were demonstrated experimentally in [51] and [57]. More recently, Floquet topological insulators were predicted to occur in photonic quasicrystalline and fractal lattices (in [52] and [53]).
55. M. Verbin, O. Zilberberg, Y. Lahini, Y. E. Kraus, and Y. Silberberg, "Topological pumping over a photonic Fibonacci quasicrystal," Phys. Rev. B **91**, 064201 (2015).
56. M. A. Bandres, M. C. Rechtsman, and M. Segev, "Topological photonic quasicrystals: fractal topological spectrum and protected transport," Phys. Rev. X **6**, 011016 (2016).
57. Z. Yang, E. Lustig, Y. Lumer, and M. Segev, "Photonic Floquet topological insulators in a fractal lattice," Light Sci. Appl. **9**, 128 (2020).
58. D. Sticlet and F. Piéchon, "Distant-neighbor hopping in graphene and Haldane models," Phys. Rev. B **87**, 115402 (2013).
59. A. Regensburger, C. Bersch, M.-A. Miri, G. Onishchukov, D. N. Christodoulides, and U. Peschel, "Parity–time synthetic photonic lattices (supplement)," Nature **488**, 167–171 (2012).

60. O. Boada, A. Celi, J. I. Latorre, and M. Lewenstein, "Quantum simulation of an extra dimension," Phys. Rev. Lett. **108**, 133001 (2012).
61. Y. E. Kraus, Y. Lahini, Z. Ringel, M. Verbin, and O. Zilberberg, "Topological states and adiabatic pumping in quasicrystals," Phys. Rev. Lett. **109**, 106402 (2012).
62. A. Celi, P. Massignan, J. Ruseckas, N. Goldman, I. B. Spielman, G. Juzeliūnas, and M. Lewenstein, "Synthetic gauge fields in synthetic dimensions," Phys. Rev. Lett. **112**, 043001 (2014).
63. D. Jukić and H. Buljan, "Four-dimensional photonic lattices and discrete tesseract solitons," Phys. Rev. A **87**, 013814 (2013).
64. S. Fishman, D. R. Grempel, and R. E. Prange, "Chaos, quantum recurrences, and Anderson localization," Phys. Rev. Lett. **49**, 509–512 (1982).
65. D. R. Grempel, R. E. Prange, and S. Fishman, "Quantum dynamics of a nonintegrable system," Phys. Rev. A **29**, 1639–1647 (1984).
66. G. Casati, I. Guarneri, and D. L. Shepelyansky, "Anderson transition in a one-dimensional system with three incommensurate frequencies," Phys. Rev. Lett. **62**, 345–348 (1989).
67. J. Chabé, G. Lemarié, B. Grémaud, D. Delande, P. Szriftgiser, and J. C. Garreau, "Experimental observation of the Anderson metal-insulator transition with atomic matter waves," Phys. Rev. Lett. **101**, 255702 (2008).
68. R. Gommers, S. Denisov, and F. Renzoni, "Quasiperiodically driven ratchets for cold atoms," Phys. Rev. Lett. **96**, 240604 (2006).
69. B. G. Klappauf, W. H. Oskay, D. A. Steck, and M. G. Raizen, "Observation of noise and dissipation effects on dynamical localization," Phys. Rev. Lett. **81**, 1203–1206 (1998).
70. H. Ammann, R. Gray, I. Shvarchuck, and N. Christensen, "Quantum delta-kicked rotor: experimental observation of decoherence," Phys. Rev. Lett. **80**, 4111–4115 (1998).
71. J. M. Edge, J. Tworzydło, and C. W. J. Beenakker, "Metallic phase of the quantum Hall effect in four-dimensional space," Phys. Rev. Lett. **109**, 135701 (2012).
72. O. Zilberberg, S. Huang, J. Guglielmon, M. Wang, K. P. Chen, Y. E. Kraus, and M. C. Rechtsman, "Photonic topological boundary pumping as a probe of 4D quantum Hall physics," Nature **553**, 59–62 (2018).
73. M. Lohse, C. Schweizer, H. M. Price, O. Zilberberg, and I. Bloch, "Exploring 4D quantum Hall physics with a 2D topological charge pump," Nature **553**, 55–58 (2018).
74. I. Petrides, H. M. Price, and O. Zilberberg, "Six-dimensional quantum Hall effect and three-dimensional topological pumps," Phys. Rev. B **98**, 125431 (2018).
75. Q. Wang, M. Xiao, H. Liu, S. Zhu, and C. T. Chan, "Optical interface states protected by synthetic Weyl points," Phys. Rev. X **7**, 031032 (2017).
76. B. K. Stuhl, H.-I.-I. Lu, L. M. Aycock, D. Genkina, and I. B. Spielman, "Visualizing edge states with an atomic Bose gas in the quantum Hall regime," Science **349**, 1514–1518 (2015).
77. M. Mancini, G. Pagano, G. Cappellini, L. Livi, M. Rider, J. Catani, C. Sias, P. Zoller, M. Inguscio, M. Dalmonte, and L. Fallani, "Observation of chiral edge states with neutral fermions in synthetic Hall ribbons," Science **349**, 1510–1513 (2015).
78. S. Kolkowitz, S. L. Bromley, T. Bothwell, M. L. Wall, G. E. Marti, A. P. Koller, X. Zhang, A. M. Rey, and J. Ye, "Spin–orbit-coupled fermions in an optical lattice clock," Nature **542**, 66–70 (2016).
79. F. A. An, E. J. Meier, and B. Gadway, "Direct observation of chiral currents and magnetic reflection in atomic flux lattices," Sci. Adv. **3**, e1602685 (2017).

80. H. Cai, J. Liu, J. Wu, Y. He, S.-Y. Zhu, J.-X. Zhang, and D.-W. Wang, "Experimental observation of momentum-space chiral edge currents in room-temperature atoms," Phys. Rev. Lett. **122**, 023601 (2019).
81. H. M. Price, T. Ozawa, and N. Goldman, "Synthetic dimensions for cold atoms from shaking a harmonic trap," Phys. Rev. A **95**, 023607 (2017).
82. X.-W. Luo, X. Zhou, C.-F. Li, J.-S. Xu, G.-C. Guo, and Z.-W. Zhou, "Quantum simulation of 2D topological physics in a 1D array of optical cavities," Nat. Commun. **6**, 7704 (2015).
83. T. Ozawa, H. M. Price, N. Goldman, O. Zilberberg, and I. Carusotto, "Synthetic dimensions in integrated photonics: from optical isolation to four-dimensional quantum Hall physics," Phys. Rev. A **93**, 043827 (2016).
84. L. Yuan, Y. Shi, and S. Fan, "Photonic gauge potential in a system with a synthetic frequency dimension," Opt. Lett. **41**, 741–744 (2016).
85. E. Lustig, S. Weimann, Y. Plotnik, Y. Lumer, M. A. Bandres, A. Szameit, and M. Segev, "Photonic topological insulator in synthetic dimensions," Nature **567**, 356–360 (2019).
86. C. W. Peterson, W. A. Benalcazar, M. Lin, T. L. Hughes, and G. Bahl, "Strong nonreciprocity in modulated resonator chains through synthetic electric and magnetic fields," Phys. Rev. Lett. **123**, 063901 (2019).
87. A. Dutt, M. Minkov, Q. Lin, L. Yuan, D. A. B. Miller, and S. Fan, "Experimental band structure spectroscopy along a synthetic dimension," Nat. Commun. **10**, 3122 (2019).
88. A. Dutt, Q. Lin, L. Yuan, M. Minkov, M. Xiao, and S. Fan, "A single photonic cavity with two independent physical synthetic dimensions," Science **367**, 59–64 (2020).
89. Q. Lin, X.-Q. Sun, M. Xiao, S.-C. Zhang, and S. Fan, "A three-dimensional photonic topological insulator using a two-dimensional ring resonator lattice with a synthetic frequency dimension," Sci. Adv. **4**, eaat2774 (2018).
90. Q. Lin, M. Xiao, L. Yuan, and S. Fan, "Photonic Weyl point in a two-dimensional resonator lattice with a synthetic frequency dimension," Nat. Commun. **7**, 13731 (2016).
91. A. Dutt, M. Minkov, I. A. D. Williamson, and S. Fan, "Higher-order topological insulators in synthetic dimensions," Light Sci. Appl. **9**, 131 (2020).
92. L. Yuan, Y. Shi, and S. Fan, "Achieving the gauge potential for the photon in a synthetic space," in *Conference on Lasers and Electro-Optics* (Optical Society of America, 2016), paper SF2E.5.
93. Z. Yang, E. Lustig, G. Harari, Y. Plotnik, Y. Lumer, M. A. Bandres, and M. Segev, "Mode-locked topological insulator laser utilizing synthetic dimensions," Phys. Rev. X **10**, 011059 (2020).
94. B. A. Bell, K. Wang, A. S. Solntsev, D. N. Neshev, A. A. Sukhorukov, and B. J. Eggleton, "Spectral photonic lattices with complex long-range coupling," Optica **4**, 1433–1436 (2017).
95. L. Yuan, Q. Lin, M. Xiao, and S. Fan, "Synthetic dimension in photonics," Optica **5**, 1396–1405 (2018).
96. Y. Wang, H. M. Price, B. Zhang, and Y. D. Chong, "Circuit implementation of a four-dimensional topological insulator," Nat. Commun. **11**, 2356 (2020).
97. L. Nemirovsky, M. Cohen, E. Lustig, and M. Segev, "Magnetic gauge field for photons in synthetic dimensions by a propagation-invariant photonic structure," in *Conference on Lasers and Electro-Optics, OSA Technical Digest* (Optical Society of America, 2009), paper FW3D.7.
98. L. Nemirovsky, M. Cohen, Y. Lumer, E. Lustig, and M. Segev, "Topological evolution-invariant photonic structures in synthetic dimensions," in *Conference*

on Lasers and Electro-Optics, OSA Technical Digest (Optical Society of America, 2020), paper FW4A.1.
99. T. Ozawa, "Artificial magnetic field for synthetic quantum matter without dynamical modulation," Phys. Rev. A **103**, 33318 (2009).
100. Y. Aharonov, L. Davidovich, and N. Zagury, "Quantum random walks," Phys. Rev. A **48**, 1687–1690 (1993).
101. E. Farhi and S. Gutmann, "Quantum computation and decision trees," Phys. Rev. A **58**, 915–928 (1998).
102. R. J. Sension, "Quantum path to photosynthesis," Nature **446**, 740–741 (2007).
103. S. Godoy and S. Fujita, "A quantum random-walk model for tunneling diffusion in a 1D lattice. A quantum correction to Fick's law," J. Chem. Phys. **97**, 5148–5154 (1992).
104. T. Oka, N. Konno, R. Arita, and H. Aoki, "Breakdown of an electric-field driven system: a mapping to a quantum walk," Phys. Rev. Lett. **94**, 100602 (2005).
105. A. Schreiber, K. N. Cassemiro, V. Potoček, A. Gábris, P. J. Mosley, E. Andersson, I. Jex, and C. Silberhorn, "Photons walking the line: a quantum walk with adjustable coin operations," Phys. Rev. Lett. **104**, 50502 (2010).
106. A. L. M. Muniz, A. Alberucci, C. P. Jisha, M. Monika, S. Nolte, R. Morandotti, and U. Peschel, "Kapitza light guiding in photonic mesh lattice," Opt. Lett. **44**, 6013–6016 (2019).
107. M. Wimmer and U. Peschel, "Observation of time reversed light propagation by an exchange of eigenstates," Sci. Rep. **8**, 2125 (2018).
108. M. Wimmer, A. Regensburger, C. Bersch, M.-A. Miri, S. Batz, G. Onishchukov, D. N. Christodoulides, and U. Peschel, "Optical diametric drive acceleration through action–reaction symmetry breaking," Nat. Phys. **9**, 780–784 (2013).
109. M. Wimmer, M.-A. Miri, D. Christodoulides, and U. Peschel, "Observation of Bloch oscillations in complex PT-symmetric photonic lattices," Sci. Rep. **5**, 17760 (2015).
110. I. D. Vatnik, A. Tikan, G. Onishchukov, D. V. Churkin, and A. A. Sukhorukov, "Anderson localization in synthetic photonic lattices," Sci. Rep. **7**, 4301 (2017).
111. M. Wimmer, A. Regensburger, M.-A. Miri, C. Bersch, D. N. Christodoulides, and U. Peschel, "Observation of optical solitons in PT-symmetric lattices," Nat. Commun. **6**, 7782 (2015).
112. A. Dikopoltsev, M. Kremer, H. H. Sheinfux, S. Weidemann, A. Szameit, and M. Segev, "Observation of Anderson localization by virtual transitions," in *Conference on Lasers and Electro-Optics* (Optical Society of America, 2020), pp. 1–2.
113. T. Kitagawa, M. S. Rudner, E. Berg, and E. Demler, "Exploring topological phases with quantum walks," Phys. Rev. A **82**, 033429 (2010).
114. T. Kitagawa, M. A. Broome, A. Fedrizzi, M. S. Rudner, E. Berg, I. Kassal, A. Aspuru-Guzik, E. Demler, and A. G. White, "Observation of topologically protected bound states in photonic quantum walks," Nat. Commun. **3**, 882 (2012).
115. F. Cardano, F. Massa, H. Qassim, E. Karimi, S. Slussarenko, D. Paparo, C. de Lisio, F. Sciarrino, E. Santamato, R. W. Boyd, and L. Marrucci, "Quantum walks and wavepacket dynamics on a lattice with twisted photons," Sci. Adv. **1**, e1500087 (2015).
116. F. Cardano, M. Maffei, F. Massa, B. Piccirillo, C. de Lisio, G. De Filippis, V. Cataudella, E. Santamato, and L. Marrucci, "Statistical moments of quantum-walk dynamics reveal topological quantum transitions," Nat. Commun. **7**, 11439 (2016).

117. S. Barkhofen, T. Nitsche, F. Elster, L. Lorz, A. Gábris, I. Jex, and C. Silberhorn, "Measuring topological invariants in disordered discrete-time quantum walks," Phys. Rev. A **96**, 033846 (2017).
118. F. Cardano, A. D'Errico, A. Dauphin, M. Maffei, B. Piccirillo, C. de Lisio, G. De Filippis, V. Cataudella, E. Santamato, L. Marrucci, M. Lewenstein, and P. Massignan, "Detection of Zak phases and topological invariants in a chiral quantum walk of twisted photons," Nat. Commun. **8**, 15516 (2017).
119. L. Xiao, X. Zhan, Z. H. Bian, K. K. Wang, X. Zhang, X. P. Wang, J. Li, K. Mochizuki, D. Kim, N. Kawakami, W. Yi, H. Obuse, B. C. Sanders, and P. Xue, "Observation of topological edge states in parity–time-symmetric quantum walks," Nat. Phys. **13**, 1117–1123 (2017).
120. S. Weidemann, M. Kremer, T. Helbig, T. Hofmann, A. Stegmaier, M. Greiter, R. Thomale, and A. Szameit, "Topological funneling of light," Science **368**, 311–314 (2020).
121. A. Schreiber, A. Gábris, P. P. Rohde, K. Laiho, M. Štefaňák, V. Potoček, C. Hamilton, I. Jex, and C. Silberhorn, "A 2D quantum walk simulation of two-particle dynamics," Science **336**, 55–58 (2012).
122. T. Nitsche, F. Elster, J. Novotný, A. Gábris, I. Jex, S. Barkhofen, and C. Silberhorn, "Quantum walks with dynamical control: graph engineering, initial state preparation and state transfer," New J. Phys. **18**, 063017 (2016).
123. B. Wang, T. Chen, and X. Zhang, "Experimental observation of topologically protected bound states with vanishing Chern numbers in a two-dimensional quantum walk," Phys. Rev. Lett. **121**, 100501 (2018).
124. H. Chalabi, S. Barik, S. Mittal, T. E. Murphy, M. Hafezi, and E. Waks, "Synthetic gauge field for two-dimensional time-multiplexed quantum random walks," Phys. Rev. Lett. **123**, 150503 (2019).
125. C. Chen, X. Ding, J. Qin, Y. He, Y.-H. Luo, M.-C. Chen, C. Liu, X.-L. Wang, W.-J. Zhang, H. Li, L.-X. You, Z. Wang, D.-W. Wang, B. C. Sanders, C.-Y. Lu, and J.-W. Pan, "Observation of topologically protected edge states in a photonic two-dimensional quantum walk," Phys. Rev. Lett. **121**, 100502 (2018).
126. J. Zak, "Berry's phase for energy bands in solids," Phys. Rev. Lett. **62**, 2747–2750 (1989).
127. P. Deymier and K. Runge, *Phase and Topology BT—Sound Topology, Duality, Coherence and Wave-Mixing: an Introduction to the Emerging New Science of Sound*, P. Deymier and K. Runge, eds. (Springer, 2017), pp. 37–80.
128. A. P. Schnyder, S. Ryu, A. Furusaki, and A. W. W. Ludwig, "Classification of topological insulators and superconductors in three spatial dimensions," Phys. Rev. B **78**, 195125 (2008).
129. C.-K. Chiu, J. C. Y. Teo, A. P. Schnyder, and S. Ryu, "Classification of topological quantum matter with symmetries," Rev. Mod. Phys. **88**, 035005 (2016).
130. C.-K. Chiu, H. Yao, and S. Ryu, "Classification of topological insulators and superconductors in the presence of reflection symmetry," Phys. Rev. B **88**, 075142 (2013).
131. T. Morimoto and A. Furusaki, "Topological classification with additional symmetries from Clifford algebras," Phys. Rev. B **88**, 125129 (2013).
132. K. Shiozaki and M. Sato, "Topology of crystalline insulators and superconductors," Phys. Rev. B **90**, 165114 (2014).
133. M. S. Rudner and L. S. Levitov, "Topological transition in a non-Hermitian quantum walk," Phys. Rev. Lett. **102**, 065703 (2009).
134. J. M. Zeuner, M. C. Rechtsman, Y. Plotnik, Y. Lumer, S. Nolte, M. S. Rudner, M. Segev, and A. Szameit, "Observation of a topological transition in the bulk of a non-Hermitian system," Phys. Rev. Lett. **115**, 040402 (2015).

135. C. Poli, M. Bellec, U. Kuhl, F. Mortessagne, and H. Schomerus, "Selective enhancement of topologically induced interface states in a dielectric resonator chain," Nat. Commun. **6**, 6710 (2015).
136. S. Weimann, M. Kremer, Y. Plotnik, Y. Lumer, S. Nolte, K. G. Makris, M. Segev, M. C. Rechtsman, and A. Szameit, "Topologically protected bound states in photonic parity–time-symmetric crystals," Nat. Mater. **16**, 433–438 (2017).
137. T. E. Lee, "Anomalous edge state in a non-Hermitian lattice," Phys. Rev. Lett. **116**, 133903 (2016).
138. D. Leykam, K. Y. Bliokh, C. Huang, Y. D. Chong, and F. Nori, "Edge modes, degeneracies, and topological numbers in non-Hermitian systems," Phys. Rev. Lett. **118**, 040401 (2017).
139. M. S. Rudner, M. Levin, and L. S. Levitov, "Survival, decay, and topological protection in non-Hermitian quantum transport," arXiv:1605.07652 (2016).
140. M. A. Bandres, S. Wittek, G. Harari, M. Parto, J. Ren, M. Segev, D. N. Christodoulides, and M. Khajavikhan, "Topological insulator laser: experiments," Science **359**, eaar4005 (2018).
141. G. Harari, M. A. Bandres, Y. Lumer, M. C. Rechtsman, Y. D. Chong, M. Khajavikhan, D. N. Christodoulides, and M. Segev, "Topological insulator laser: theory," Science **359**, eaar4003 (2018).
142. H. Shen, B. Zhen, and L. Fu, "Topological band theory for non-Hermitian Hamiltonians," Phys. Rev. Lett. **120**, 146402 (2018).
143. X. Chen, Z.-C. Gu, Z.-X. Liu, and X.-G. Wen, "Symmetry-protected topological orders in interacting bosonic systems," Science **338**, 1604–1606 (2012).
144. M. E. Tai, A. Lukin, M. Rispoli, R. Schittko, T. Menke, D. Borgnia, P. M. Preiss, F. Grusdt, A. M. Kaufman, and M. Greiner, "Microscopy of the interacting Harper–Hofstadter model in the two-body limit," Nature **546**, 519–523 (2017).
145. S. de Léséleuc, V. Lienhard, P. Scholl, D. Barredo, S. Weber, N. Lang, H. P. Büchler, T. Lahaye, and A. Browaeys, "Observation of a symmetry-protected topological phase of interacting bosons with Rydberg atoms," Science **365**, 775–780 (2019).
146. Y. Tenenbaum Katan, R. Bekenstein, M. Bandres, Y. Lumer, Y. Plotnik, and M. Segev, "Induction of topological transport by long ranged nonlinearity," in *Conference on Lasers and Electro-Optics*, OSA Technical Digest (online) (2016), paper FM3A.6.
147. L. J. Maczewsky, M. Heinrich, M. Kremer, S. K. Ivanov, M. Ehrhardt, F. Martinez, Y. V. Kartashov, V. V. Konotop, L. Torner, D. Bauer, and A. Szameit, "Nonlinearity-induced photonic topological insulator," Science **370**, 701–704 (2020).
148. N. P. Mitchell, L. M. Nash, D. Hexner, A. M. Turner, and W. T. M. Irvine, "Amorphous topological insulators constructed from random point sets," Nat. Phys. **14**, 380–385 (2018).
149. S. Aubry and G. André, "Analyticity breaking and Anderson localization in incommensurate lattices," Ann. Isr. Phys. Soc. **3**, 133–140 (1980).
150. C. H. Lee, Y. Wang, Y. Chen, and X. Zhang, "Electromagnetic response of quantum Hall systems in dimensions five and six and beyond," Phys. Rev. B **98**, 094434 (2018).
151. R. B. Laughlin, "Quantized Hall conductivity in two dimensions," Phys. Rev. B **23**, 5632–5633 (1981).
152. B. A. Bernevig and S.-C. Zhang, "Quantum spin Hall effect," Phys. Rev. Lett. **96**, 106802 (2006).
153. A. Cerjan, M. Wang, S. Huang, K. P. Chen, and M. C. Rechtsman, "Thouless pumping in disordered photonic systems," Light Sci. Appl. **9**, 178 (2020).

154. F. Zangeneh-Nejad and R. Fleury, "Zero-index Weyl metamaterials," Phys. Rev. Lett. **125**, 054301 (2020).
155. X. Zhang, K. Ding, X. Zhou, J. Xu, and D. Jin, "Experimental observation of an exceptional surface in synthetic dimensions with Magnon polaritons," Phys. Rev. Lett. **123**, 237202 (2019).
156. Q. Wang, K. Ding, H. Liu, S. Zhu, and C. T. Chan, "Exceptional cones in 4D parameter space," Opt. Express **28**, 1758–1770 (2020).
157. L. J. Maczewsky, K. Wang, A. A. Dovgiy, A. E. Miroshnichenko, A. Moroz, M. Ehrhardt, M. Heinrich, D. N. Christodoulides, A. Szameit, and A. A. Sukhorukov, "Synthesizing multi-dimensional excitation dynamics and localization transition in one-dimensional lattices," Nat. Photonics **14**, 76–81 (2020).
158. C. Qin, F. Zhou, Y. Peng, D. Sounas, X. Zhu, B. Wang, J. Dong, X. Zhang, A. Alù, and P. Lu, "Spectrum control through discrete frequency diffraction in the presence of photonic gauge potentials," Phys. Rev. Lett. **120**, 133901 (2018).
159. Z.-D. Cheng, Q. Li, Z.-H. Liu, F.-F. Yan, S. Yu, J.-S. Tang, Z.-W. Zhou, J.-S. Xu, C.-F. Li, and G.-C. Guo, "Experimental implementation of a degenerate optical resonator supporting more than 46 Laguerre-Gaussian modes," Appl. Phys. Lett. **112**, 201104 (2018).
160. A. Perez-Leija, R. Keil, A. Kay, H. Moya-Cessa, S. Nolte, L.-C. Kwek, B. M. Rodríguez-Lara, A. Szameit, and D. N. Christodoulides, "Coherent quantum transport in photonic lattices," Phys. Rev. A **87**, 012309 (2013).
161. E. Lustig, L. Maczewsky, T. Biesenthal, Z. Yang, Y. Plotnik, A. Szameit, and M. Segev, "Experimentally realizing photonic topological edge states in 3D," in *Conference on Lasers and Electro-Optics*, OSA Technical Digest (Optical Society of America, 2020), paper FW3A.2.
162. And, therefore, it has the same topological bandgap and bands in both representations. Since the transformation between synthetic space and real space is a unitary transformation, the dispersion of the system is preserved between the synthetic space and real space.
163. G. Harari, M. A. Bandres, Y. Lumer, Y. Plotnik, D. N. Christodoulides, and M. Segev, "Topological lasers," in *Conference on Lasers and Electro-Optics* (Optical Society of America, 2016), paper FM3A.3.
164. B. Bahari, A. Ndao, F. Vallini, A. El Amili, Y. Fainman, and B. Kanté, "Nonreciprocal lasing in topological cavities of arbitrary geometries," Science **358**, 636–640 (2017).
165. Y. Zeng, U. Chattopadhyay, B. Zhu, B. Qiang, J. Li, Y. Jin, L. Li, A. G. Davies, E. H. Linfield, B. Zhang, Y. Chong, and Q. J. Wang, "Electrically pumped topological laser with valley edge modes," Nature **578**, 246–250 (2020).
166. I. Amelio and I. Carusotto, "Theory of the coherence of topological lasers," Phys. Rev. X **10**, 041060 (2019).
167. Y. G. N. Liu, P. Jung, M. Parto, W. E. Hayenga, D. N. Christodoulides, and M. Khajavikhan, "Topological Haldane lattice," in *Conference on Lasers and Electro-Optics* (Optical Society of America, 2020), paper FW3A.1.
168. K. Wang, A. Dutt, K. Y. Yang, C. C. Wojcik, J. Vučković, and S. Fan, "Generating arbitrary topological windings of a non-Hermitian band," Science **371**, 1240–1245 (2021)
169. M. Segev, Y. Ophir, B. Fischer, and G. Eisenstein, "Mode locking and frequency tuning of a laser diode array in an extended cavity with a photorefractive phase conjugate mirror," Appl. Phys. Lett. **57**, 2523–2525 (1990).
170. L. Yuan, A. Dutt, M. Qin, S. Fan, and X. Chen, "Creating locally interacting Hamiltonians in the synthetic frequency dimension for photons," Photon. Res. **8**, B8–B14 (2020).

171. C. Joshi, A. Farsi, A. Dutt, B. Y. Kim, X. Ji, Y. Zhao, A. M. Bishop, M. Lipson, and A. L. Gaeta, "Frequency-domain quantum interference with correlated photons from an integrated microresonator," Phys. Rev. Lett. **124**, 143601 (2020).
172. A. K. Tusnin, A. M. Tikan, and T. J. Kippenberg, "Nonlinear states and dynamics in a synthetic frequency dimension," Phys. Rev. A **102**, 023518 (2020).
173. K. Wang, B. A. Bell, A. S. Solntsev, D. N. Neshev, B. J. Eggleton, and A. A. Sukhorukov, "Multidimensional synthetic chiral-tube lattices via nonlinear frequency conversion," Light Sci. Appl. **9**, 132 (2020).
174. I. Martin, G. Refael, and B. Halperin, "Topological frequency conversion in strongly driven quantum systems," Phys. Rev. X **7**, 041008 (2017).
175. L. Yuan, M. Xiao, Q. Lin, and S. Fan, "Synthetic space with arbitrary dimensions in a few rings undergoing dynamic modulation," Phys. Rev. B **97**, 104105 (2018).
176. E. Lustig, Y. Sharabi, and M. Segev, "Topological aspects of photonic time crystals," Optica **5**, 1390–1395 (2018).
177. N. H. Lindner, G. Refael, and V. Galitski, "Floquet topological insulator in semiconductor quantum wells," Nat. Phys. **7**, 490–495 (2011).
178. G. Puentes and O. Santillán, "Zak phase in discrete-time quantum walks," arXiv:1506.08100v2 (2015).
179. J. Boutari, A. Feizpour, S. Barz, C. D. Franco, M. Kim, W. S. Kolthammer, and I. A. Walmsley, "Large scale quantum walks by means of optical fiber cavities," J. Opt. **18**, 94007 (2016).
180. M. S. Rudner, N. H. Lindner, E. Berg, and M. Levin, "Anomalous edge states and the bulk-edge correspondence for periodically driven two-dimensional systems," Phys. Rev. X **3**, 031005 (2013).

Eran Lustig is a Ph.D. student at the Technion—Israel Institute of Technology. He received his B.Sc. in physics and a B.Sc. in electrical engineering at the Technion. He is the recipient of the Leonard and Diane Sherman Interdisciplinary Graduate School Fellowship (2016) and the recipient of the prestigious Adams fellowship for doctoral students for outstanding Israeli doctoral students in the exact sciences. In his research, he studies theoretically and experimentally the propagation of light in non-spatial dimensions, and he takes interest in using machine learning approaches in experimental physics.

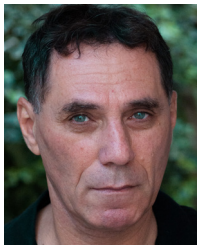

Moti Segev is the Robert J. Shillman Distinguished Professor of Physics and Electrical Engineering at the Technion, Israel. He received his B.Sc. and Ph.D. from the Technion in 1985 and 1990. After his postdoc at Caltech, he joined Princeton as Assistant Professor (1994), becoming Associate Professor in 1997 and Professor in 1999. Subsequently, Moti went back to Israel, and in 2009 he was appointed as Distinguished Professor (highest academic rank at the Technion). Moti's interests are mainly in nonlinear optics, photonics, solitons, sub-wavelength imaging, lasers, quantum simulators, and quantum electronics, although he finds entertainment in more demanding fields such as basketball and hiking. He has won numerous international awards, among them the 2007 Quantum Electronics Prize of the European Physics Society, the 2009 Max Born Award of the The Optical Society, and the 2014 Arthur Schawlow Prize of the American Physical Society. In 2011, he was elected to the Israel Academy of Sciences and Humanities, and in 2015 he was elected to the National Academy of

Science (NAS) of the United States of America. In 2014, Moti Segev won the Israel Prize in Physics and Chemistry (highest honor in Israel), and in 2019 he won the EMET Prize (Israel). However, above all his personal achievements, he takes pride in the success of his graduate students and postdocs; among them are currently 23 professors in the USA, Germany, Taiwan, Croatia, Italy, India, China, and Israel, and many hold senior R&D positions in the industry.